Journal of Molecular Structure 1244 (2021) 130965

Contents lists available at ScienceDirect

Journal of Molecular Structure

journal homepage: www.elsevier.com/locate/molstr

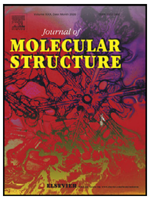

Experimental and theoretical insights into the photophysical and electrochemical properties of flavone-based hydrazones

Meshari A. Alsharif[a], Nafeesa Naeem[b], Ehsan Ullah Mughal[b,*], Amina Sadiq[c], Rabab.S. Jassas[d], Samia Kausar[a], Ataf Ali Altaf[e], Muhammad Naveed Zafar[f], Amara Mumtaz[g], Rami J. Obaid[a], Reem I. Alsantali[h], Safeer Ahmed[f], Ishtiaq Ahmed[i], Hatem M. Altass[a], Saleh A. Ahmed[a,j,k,*]

[a] *Department of Chemistry, Faculty of Applied Science, Umm Al-Qura University, 21955 Makkah, Saudi Arabia*
[b] *Department of Chemistry, University of Gujrat, Gujrat 50700, Pakistan*
[c] *Department of Chemistry, Govt. College Women University, Sialkot 51300, Pakistan*
[d] *Department of Chemistry, Jamoum University College, Umm Al-Qura University, 21955 Makkah, Saudi Arabia*
[e] *Department of Chemistry, University of Okara, Okara 56300, Pakistan*
[f] *Department of Chemistry, Quaid-i-Azam University, Islamabad 45320, Pakistan*
[g] *Department of Chemistry, COMSATS University Islamabad, Abbottabad, Pakistan*
[h] *Department of Pharmaceutical Chemistry, Pharmacy College, Taif University, 888 Taif, Saudi Arabia*
[i] *Department of Engineering & Biotechnology, University of Cambridge, Cambridge, United Kingdom*
[j] *Research Laboratories Unit, Faculty of Applied Science, Umm Al-Qura University, 21955 Makkah, Saudi Arabia*
[k] *Chemistry Department, Faculty of Science, Assiut University, 71516 Assiut, Egypt*

ARTICLE INFO

Article history:
Received 26 April 2021
Revised 19 June 2021
Accepted 21 June 2021
Available online 24 June 2021

Keywords:
Flavone hydrazones
UV–vis spectroscopy
Fluorescence spectroscopy
Cyclic voltammetry
Structure-property relationship
Density functional theory

ABSTRACT

A small library of flavone-based hydrazones has been designed, synthesized and characterized. In this context, thirteen flavone hydrazones **(3a-3 m)** were synthesized by the acid-catalyzed condensation of flavone with 2,4-dinitrophenylhydrazine (2,4-DNPH) and characterized by different spectral techniques (IR, UV–Vis, NMR and mass spectrometry). The electrochemical, photophysical and theoretical investigations of such type of compounds are hitherto unknown. The electrochemical behavior of these hydrazones at a platinum electrode has been analyzed by cyclic voltammetry (CV) and was investigated at 200, 100 and 40 mVs^{-1} in acetonitrile (CH_3CN). These hydrazones showed a quasi-reversible redox reaction. The oxidation–reduction reactive sites of these derivatives were located *via* geometry optimization using density functional theory (DFT) at the B3LYP/3–21 g in the Guassian-09 level of theory. Moreover, the target compounds exhibited interesting fluorescent properties. Owing to their excellent photophysical and redox results, a detailed structure-property relationship was established to assess the substituents impact and their position on the physicochemical and electronic properties. All the experimental results were in accordance with the computational studies.

1. Introduction

The innovations in the research area have revealed many secret zones that can resolve many known challenges of the advanced world. Synthetic substances along with naturally originated substances that show elevated anti-oxidative activity are attracting high consideration. Many accomplishments have been achieved in electrochemistry such as obtaining qualitative and quantitative information about electrochemical reactions.' 'Among several organic molecular systems, the hydrazone (-C=N–NH-) linkage in compounds has significant nonlinear optical sensitivity due to their architectural flexibility. Hydrazones are versatile molecules and have received considerable interest in research both fundamental and application.

Flavone (Fig. 1) is one of the subclasses of the flavonoid family that is present in dietary components found in herbs, cereals, vegetables and fruits [1–7]. To discover the varied functions of 2-phenylchromone (flavone), exploring different synthetic methods and structural variation has now become an essential goal of some research groups [8,9]. Thus, synthetically acquired flavone scaffold having a range of bioactivities can be taken as lead [21] compounds for the hydrazones syntheses with various distinct func-

---

* Correspondinag authors.
E-mail addresses: ehsan.ullah@uog.edu.pk (E.U. Mughal), saahmed@uqu.edu.sa (S.A. Ahmed).

https://doi.org/10.1016/j.molstruc.2021.130965

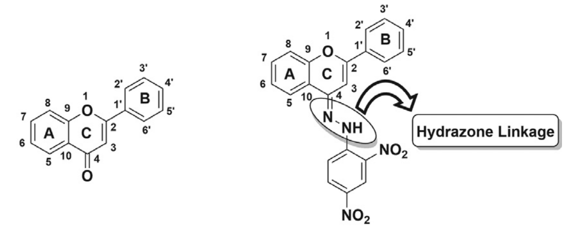

2-Phenyl-4*H*-chromen-4-one
(Flavone)
(a)

(2,4-Dinitrophenyl)-2-(2-phenyl-4*H*-chromen-4-ylidene)hydrazine
(Flavone hydrazone)
(b)

Fig. 1. Representative structures of **(a)** = Flavone, **(b)** = Flavone hydrazone.

tional groups at the 4′-position of flavone skeleton [9a–9c]. The search for novel therapeutic and electrochemical agents directed scientists' attention to Schiff base (azomethines) hydrazones formation.

Schiff bases are recognized as a versatile class of compounds that have significant properties and an extensive range of applications in catalysts, dyes, pigments, chemosensors and intermediates in organic synthesis [10].

Flavone hydrazones (Fig. 1) are a chemical family of one of the Schiff bases, nitrogen compounds, whose existence in nature has been reported [11, 12]. Azomethines are the most prevalent and frequently used organic compounds in many domains and play an essential role in pharmacology and materials chemistry [13–16]. Because of the existence of fundamental sites such as heteroatoms like 'O' and 'N', these ligands could form complexes by donating their non-bonding electron pairs, thus leading to the high stability of compounds [17, 18].

Fluorescent studies reveal the worth of the pi-electrons rich organic materials as excellent molecules for use in analytical sensors, electrochromic devices and light-emitting diodes [19, 20][21]. In this context, the azomethine ($-HC{=}N-$) functionality has received significant concern because of its distinctive properties such as auto-fluorescent property attributing to $n{\rightarrow}\pi^*$ transition of the C=N bond, and the extensive π-conjugation system [21a]. Organic fluorescent molecules are believed to be superior as compared to inorganic ones due to their wide range of $\lambda_{\text{emission}}$ and high luminous productivity. The designing of new organic luminogens is developing as a dynamic study that suggests an economical color purity, ease of synthesis, purification, liquid state emission and electrochemical stability in organic light-emitting diodes (OLEDs) [21b]. Schiff bases give several benefits, *e.g.*, prolonged incandescent excited states and photochemical strengths [22]. Moreover, the core-functionalization of hydrazone analogs with EDGs and EWGs has not been used as considerably as potential fluorescent probes. The reports showed that electron-donating and -accepting groups can be employed to alter the physicochemical and redox properties of hydrazones.

Furthermore, the electrochemical studies offer an immense quantity of indication concerning the mechanism of bio-electron charge transfer and are used to determine the analog's impact on redox behavior [23, 24]. Cyclic voltammetry (CV) is an extensively used voltammetric technique that allows determining the oxidation–reduction behavior of compounds in the solution form [25–28]. The electrochemical oxidation and reduction processes of flavonolic compounds have been investigated using this technique. The purpose of the current study was to use CV to assess the electrochemical behavior of various flavone hydrazones [29–33]. Thus, to acquire more information of the structure-property correlations (emission, absorption and redox properties), a number of different donor- and acceptor- functional groups were introduced at 4′-position of the flavone hydrazone skeleton.

The modern research developments, particularly in synthetic chemistry, have coincided with computations to explore numerous structural features of synthesized analogs [34]. DFT is now becoming a prominent method for its beneficial intuitions to distinguish key evidence around the mechanism and stability of novel targeted derivatives. These computational calculations are very important in recognizing the possible reactive sites of synthesized molecules, which are susceptible to nucleophilic or electrophilic attacks, as these sites enhance the physiochemical and electrochemical properties of potent compounds [35, 36].

There is sufficient literature available on the UV, emission and redox behavior of different heterocycles [37–40], however, to the best of our knowledge, there is no literature available on the photophysical and electrochemical properties of flavone-based hydrazones.

Considering the above-mentioned reports and our continued interest in the development of novel flavone hydrazone analogs, herein, we report the design, synthesis and evaluation of flavone-based hydrazones for their photophysical and electrochemical properties studies. The experimental results were validated by a computational approach. In addition, we tried to explain the structure-property relationship in detail.

2. Material and methods

Most of the starting materials, solvents and chemicals were bought from Sigma-Aldrich and were utilized as received. Electrothermal digital instrument was used to access the melting points and are uncorrected. A Bio-Rad spectrophotometer has been used to record the IR spectra. NMR spectra were obtained using a Bruker spectrometer (^{1}H, 600 MHz, ^{13}C, 151 MHz). NMR chemical shift values were defined in δ (ppm) units. The reaction completion was observed by TLC and spots were visualized under a UV lamp (254 nm). The QUARTZ cell was used to record the absorption spectra in CH_3CN on the Jasco UV–VIS V-660 instrument. Steady-state fluorescence measurements were carried out on a Shimadzu RF-6000 Spectro fluorophotometer. Cyclic voltammetry (CV) was performed with a typical three-electrode arrangement consisting of a reference electrode (Ag/AgCl), auxiliary electrode (platinum wire), and the working electrode (glassy carbon). The cyclic voltammograms have been recorded in acetonitrile (CH_3CN) in 0.1 M TBAB as the supporting electrolyte with a scan rate ranging from −2.0 to 1.0 Vs^{-1}, using a CHI620 C model electrochemical potentiostat instrument at ambient temperature.

*2.1. Procedure for the synthesis of chalcones (**1a-1 m**) [9d], flavones (**2a-2 m**) [9d] and flavone hydrazones (**3a-3 m**) [9a]*

A solution of 2′-hydroxyacetophenone (0.12 mL, 1.0 mmol), aq. sodium hydroxide solution (10 mL) (30%) was dissolved in MeOH (25.0 mL) and stirred for 30 min at room temperature with the subsequent addition of various aryl aldehyde (1.0 mmol) dropwise at the same temperature, the reaction mixture was stirred for further 4 h. 'The reaction mixture progress was observed by TLC using a mixture of ethyl acetate: *n*-hexane (1:3) as a mobile phase. After the completion of the reaction, the reaction mixture was acidified with dilute HCl (10%). The precipitated solid was filtered, washed with distilled H_2O and ultimately recrystallized from EtOH to get the purified product. Subsequently, the substituted chalcone (1.0 mmol), was dissolved in DMSO (10 mL) and oxidatively cyclized in the presence of a small amount of iodine I_2 (254 mg, 1.0 mmol). The reaction mixture was refluxed at 130–140 °C on an oil bath for 4–5 hours. Afterwards, the reaction mixture was poured onto the crushed ice, the resulting solid was treated with a solution of 10% $Na_2S_2O_3$ to get rid of unreacted I_2, finally with distilled H_2O and recrystallized from EtOH to get a purified product.

The obtained substituted flavone and 2,4-dinitrophenylhydrazine (DNPH) were dissolved in EtOH (15 mL). To this mixture, 3–4 drops of concentrated sulfuric acid (H_2SO_4) were added and allowed the mixture to reflux for 4 h. Upon cooling and diluting with ice-cold water, an intense colored solid mass separated out, which was further recrystallized from ethanol to give the desired product.

2.2. UV–Vis measurement

The UV–Visible absorption spectra have been obtained using a Jasco UV–Vis V-660 spectrophotometer in 200 to 800 nm wavelength range. The samples were prepared at a concentration of 0.1 mmol/L using acetonitrile (CH_3CN) as a solvent [41]. The faster the electrons are stimulated, the longer they can absorb the wavelength of light. The instrument works by passing a beam of light through a sample and measuring the wavelength of light to the detector. Synthesized hydrazone derivatives can exhibit a variety of transitions; π-π^*, n-π^*, σ-σ^*, n-σ^*, due to the presence of σ and π bond and lone pair of electrons on 'N' atoms of flavone moiety. Characteristically, the most favored transition is from the HOMO to the LUMO. The UV light absorbed by a molecule can create a distinct spectrum that helps to identify the product.

2.3. Fluorescence measurement

The fluorescence spectra of hydrazones were examined using Shimadzu RF-6000 Spectro fluorophotometer equipped with a 450 W Xe laser lamp as the excitation source. Concentration of 1×10^{-3} M of the compound, soluble in CH_3CN, has been used to measure the fluorescence spectra of hydrazones at ambient temperature with 320 nm excitation wavelength [41].

2.4. FTIR measurements

Nicolet FT-IR Impact 400D infrared spectrometer was used for recording IR spectra of the solid samples by the matrix of KBr in the range of 500–4000 cm^{-1} [41]. Each sample was ground with spectroscopic grade potassium bromide (KBr) powder and then pressed into 1 mm pellets (2 mg of sample per 200 mg dry KBr). A blank KBr disk was used as background. FT-IR spectra were smoothed, and the baseline was corrected automatically using the spectrophotometer's built-in software (Spectra Manager^{TM} II, JASCO Corporation).

2.5. Cyclic voltammetry

Electrochemical measurements have been performed out on a Model CHI620 C electrochemical analyzer, in a conventional 3-electrode electrochemical cell with Pt wire as counter-electrode, glassy carbon as a working electrode and Ag/AgCl (3 M KCl) as the reference electrode in acetonitrile (CH_3CN). The electrode reactions that characterize the electrochemical oxidation of flavone hydrazones at the glassy carbon electrode (GCE) were studied using the CV method. TBAB was used as a supporting electrolyte. The concentration of the sample run was 0.1 mM in CH_3CN. The cyclic voltammograms were recorded at a scan rate of 200, 100 and 40 mVs^{-1} in the potential range from -2.0 to $+1.0$ V. The curves were scanned from the most negative potential about -2.0 V towards a more positive direction up to about 1.0 V. All the experiments were carried out at ambient temperature [13, 42].

2.6. Computational (DFT) calculations

DFT calculations were performed for synthesized electroactive analogs to accompany the experimental findings of CV. The redox potentials of the desired derivatives measured from CV showed a similar pattern to that predicted from the DFT work [43]. DFT computations were carried out by using DFT-B3LYP/3–21 g in Guassian-09 [44]. The ground states geometries of representative analogs **(3a-3j)** were optimized using hybrid functional B3LYP and basis set 3–21 g. B3LYP functional combined to 3–21 g basis set includes exact exchange and GGA corrections along with LDA electron-electron and electron-nuclei energy. So, this hybrid exchange functional is the simplest parameter to reproduce the geometry of a test suite of organic molecules as per literature reports [41, 43, 50]. TD-DFT calculations were performed at B3LYP/321 g level to calculate the UV-Visible spectra whereas vibrational analysis was carried out by using Freq-DFT/B3LYP/321 g and these theoretical results were compared with experimental results. The VEDA 4 program has been used to perform different vibrational parameters and PED calculations [51].

3. Results and discussion

3.1. Chemistry

The synthetic method applied for the synthesis of hydrazones (**3a-3 m**) is depicted in Scheme 1. Initially, 2′-hydroxyacetophenone undergoes Claisen-Schmidt condensation with variously substituted aryl aldehydes using aqueous NaOH in methanol to form the substituted intermediate chalcones **(1a-1 m).** These chalcones were then oxidatively cyclized to yield flavones **(2a-2 m)** using a well-known I_2-DMSO mixture as the oxidizing agent. These flavone derivatives were purified via recrystallization by EtOH and analyzed by IR, NMR and UV–Vis spectroscopy only. The targeted hydrazones **(3a-3 m)** were synthesized through condensation of flavones with 2,4-dinitrophenylhydrazine (2,4-DNPH) in the presence of conc. H_2SO_4 and absolute EtOH under reflux conditions. The expected final products (Scheme 1) were isolated as solid materials in moderate to excellent yields. The synthesized target molecules **(3a-3 m)** were further purified through recrystallization in EtOH and found quite stable at ambient conditions. These desired analogs are dissolve in common organic solvents such as DMSO, CH_3CN and DMF, etc. The chemical structures of all the newly synthesized flavone hydrazones were corroborated by IR, UV–Vis and NMR spectroscopic techniques. For instance, the disappearance of an absorption band around 1655 cm^{-1} and the appearance of a new peak around 1615 cm^{-1} in IR spectra clearly indicates the conversion of the carbonyl group ($C = O$) into azomethine linkage ($C = N$) along with other characteristics N–H *str.* vibration band around 3350 cm^{-1}. Their UV–Vis measurements were taken in CH_3CN solution. The absorption bands in the range of 300–350 nm are expectedly due to $\pi \rightarrow \pi*$ and $n \rightarrow \pi*$ transitions in imine ($C = N$) group, whereas the bands in 200–400 nm range can be related to $\pi \rightarrow \pi*$ transitions of the aromatics. Likewise, ^1H NMR spectra indicate a highly downfield singlet around δ 11.55 ppm and doublet ($J = 6.0$ Hz) in the range of δ 8.81–8.86 ppm for N–H and the most deshielded aromatic proton respectively. Additionally, proton NMR spectra also show a characteristic singlet for the proton at position-3 (flavone skeleton) in the range of δ 7.00–7.10 ppm. The rest of the signals in the range of 7.00–8.00 ppm are related to the aromatic protons of rings A & B of the flavone structure. Similarly, there is the appearance of a new signal around δ 160.0 ppm for $C = N$ bond in the ^{13}C NMR spectra. The NMR peaks around 155, 147 and 145 ppm, etc. are assigned to the 2,4-DNPH part of the hydrazones. Whereas, the chemical shift values present in the range of 135–120 ppm are related to aromatic carbons. Furthermore, the molecular masses of all the newly synthesized hydrazones were verified by EI-MS, and thus all the spectroscopic data are good in agreement with the proposed structures of the desired flavone hydrazones.

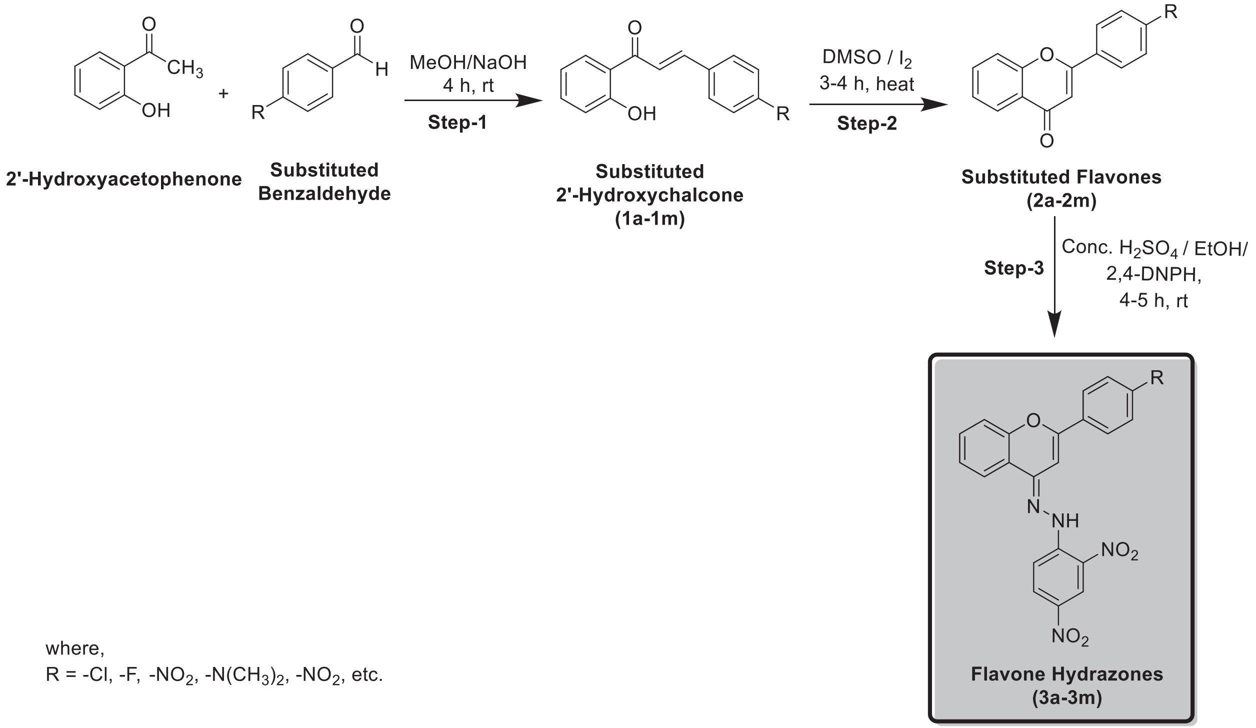

Compound No.	Structural formula	Compound No.	Structural formula
3a.	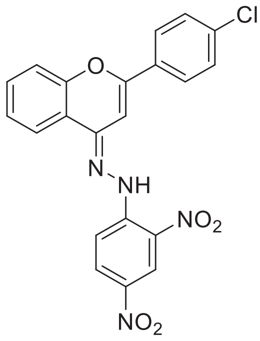	**3h.**	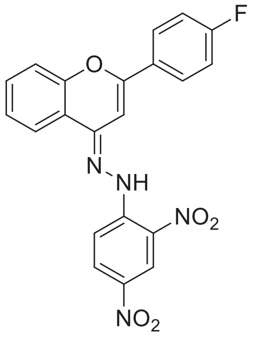

Scheme 1. Synthesis of flavone hydrazones **(3a-3 m)**.

The spectroscopic data of already reported 2′-hydroxychalcones **(1a-1 m)** and **1a, 1b, 1f, 1 h** [9d]; **1c** [9e]; **1d, 1k** and **1l** [9f]; **1e** [9 g]; **1 g** [9h]; **1i** [9i]; **1 m** [9j] and substituted flavones **(2a-2 m) 2a, 2b, 2f** and **2 h** [9d]; **2c, 2 g** [9k]; **2d** [9l]; **2e** [9m]; **2i, 2k** [9n]; **2l** [9o]; **2 m** [9p]; have been given in literature as cited above. Also, the spectral data of reported hydrazone compounds **3b, 3c, 3f, 3 h** and **3k** have been mentioned in the literature [9a].

3.1.1. *1-(2-Hydroxyphenyl)–3-(1-tosyl-1H-indol-2-yl)prop–2-en-1-one (1j)*

Light-orange solid; Yield: 84%; M.P. 137–139 °C; $R_f = 0.5$; UV–Vis λ_{max} (CH_3CN) = 376 nm; λ_{em} (CH_3CN) = 580 nm; FTIR (cm^{-1}): 3083 (aromatic C–H str.), 1655 (s, $C = O$ str., α,β unsaturated, aliphatic), 1576 (m, aliphatic $C = C$ str.), 1540 (aromatic), 1280 (C–O str.), 659 (C-indole); ^1H NMR (600 MHz, DMSO–d_6): δ 13.80 (bs, 1H, OH), 8.46 (s, 1H, Ar-H), 8.40–8.30 (m, 2H, Ar-H), 8.15–7.99 (m, 3H, Ar-H), 7.85 (s, 2H, -CH=CH-), 7.68 (d, J = 12.0 Hz, 2H, Ar-H), 7.43–7.25 (m, 1H, Ar-H), 7.22 (d, J = 12.0 Hz, 2H, Ar-H), 7.00–6.90–6.70 (m, 2H, Ar-H), 2.30 (s, 3H, CH_3); ^{13}C NMR (151 MHz, DMSO–d_6): δ 191.4, 162.2, 154.7, 147.8, 145.0, 142.2, 138.1, 136.0, 132.2, 131.0, 130.4, 128.5, 125.1, 124.0, 123.1, 120.6, 120.0, 118.8, 118.1, 116.2, 115.4, 114.2, 110.7, 21.5; accurate mass (EI-MS) of $[M]^{+\bullet}$: Calcd. for $C_{24}H_{19}NO_4S$ 417.10348; found 417.10333.

3.1.2. *2-(1-Tosyl-1H-indol-3-yl)–4H-chromen-4-one (2j)*

Light-yellow solid; Yield: 77%; M.P. 135–137 °C; $R_f = 0.6$; UV–Vis λ_{max} (CH_3CN) = 332 nm; λ_{em} (CH_3CN) = 680 nm; FTIR (cm^{-1}): 3089 (aromatic C–H str.), 1672 (s, $C = O$ str.), 1450 (m, aromatic $C = C$ str.), 1255 (C–O str.), 679 (*p*-monosubstituted); ^1H NMR (600 MHz, DMSO–d_6): δ 8.40 (s, 1H, Ar-H), 8.35 (d, J = 6.0 Hz, 1H, Ar-H), 8.10 (d, J = 6.0 Hz, 1H, Ar-H), 7.99–7.95 (m, 2H, Ar-H), 7.75 (d, J = 12.0 Hz, 1H, Ar-H), 7.50 (d, J = 12.0 Hz, 2H, Ar-H), 7.32–7.20 (m, 1H, Ar-H), 7.19 (d, J = 12.0 Hz, 2H, Ar-H), 7.18 (s, 1H, -$C = C$–H), 7.00–6.90 (m, 1H, Ar-H), 6.90 (d, J = 12.0 Hz, 1H, Ar-H), 2.27 (s, 3H, CH_3); ^{13}C NMR (151 MHz, DMSO–d_6): δ 171.1, 161.2, 154.7, 147.6, 144.7, 142.0, 137.8, 135.4, 132.0, 131.2, 130.0, 128.7, 125.0, 124.3, 123.4, 120.3, 120.1, 119.1, 118.0, 116.0, 115.5, 114.3, 110.8, 21.4; accurate mass (EI-MS) of $[M]^{+\bullet}$: Calcd. for $C_{24}H_{17}NO_4S$ 415.07218; found 415.07207.

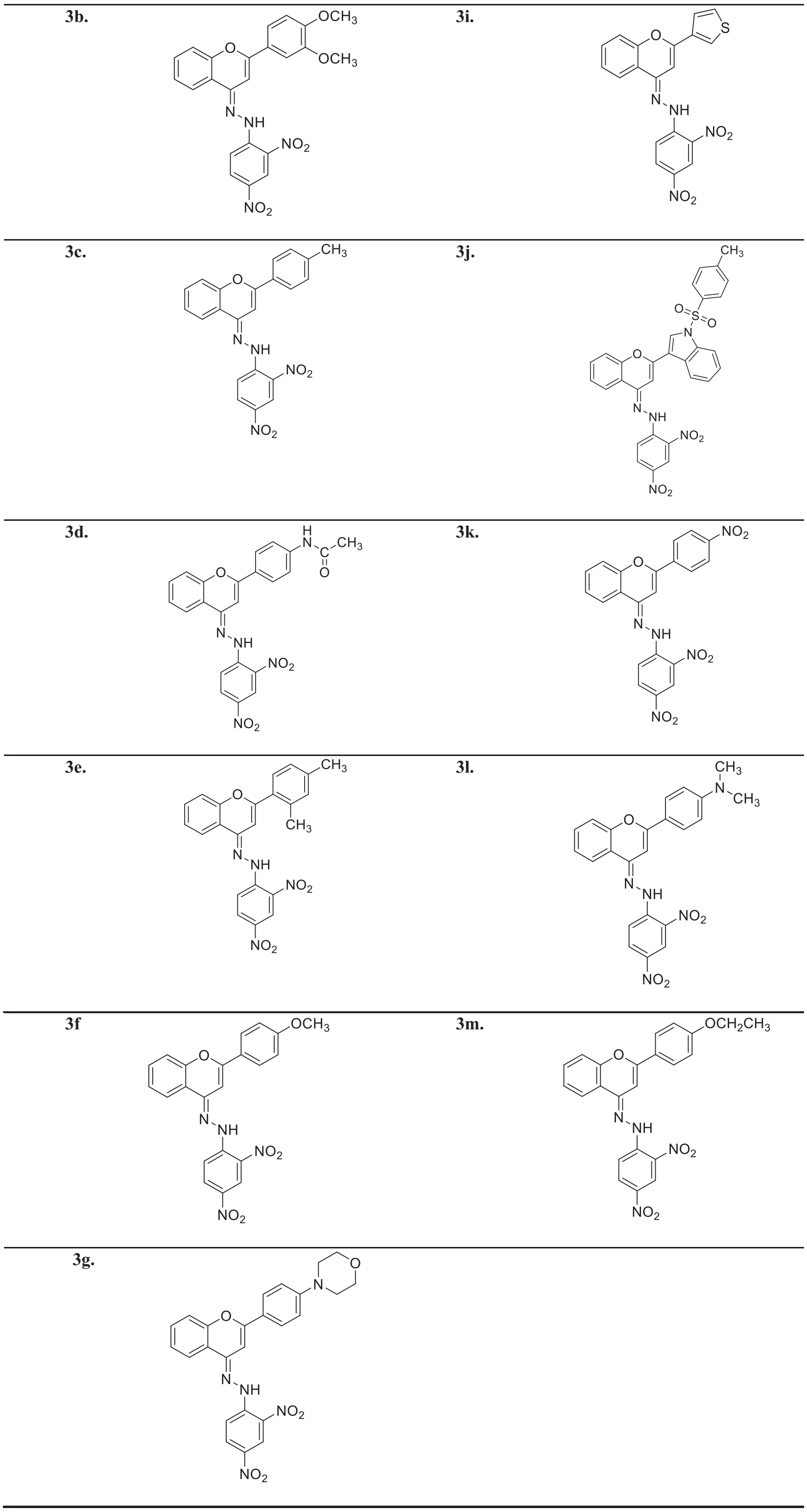

Scheme 1. Continued

3.1.3. 1-(2-(4-Chlorophenyl)–4H-chromen-4-ylidene)–2-(2,4-dinitrophenyl) hydrazine (3a)

Maroon-colored powder; Yield: 85%; M.P. 199–201 °C; $R_f = 0.8$; UV–Vis λ_{max} (CH_3CN) = 290, 358 nm; λ_{em} (CH_3CN) = 378, 717 nm; FTIR (cm^{-1}): 3362 (N–H str.), 3102 (aromatic C–H str.), 1613 (s, $C = N$ str.), 1573 (m, aromatic $C = C$ str.), 1511 (C–NO_2 asym.), 1375 (C–NO_2 sym.), 1330 (C–N str.), 1251 (C–O str.), 763 (C–Cl str.), 752 (*p*-monosubstituted); ^{1}H NMR (600 MHz, DMSO–d_6): δ 11.56 (s, 1H, -$N = N$–H), 8.86 (d, $J = 6.0$ Hz, 1H, Ar-H), 8.44 (dd, $J = 12.0$, 6.0 Hz, 1H, Ar-H), 8.05 (d, $J = 12.0$ Hz, 1H, Ar-H), 7.95 (d, $J = 12.0$ Hz, 2H, Ar-H), 7.65 (d, $J = 12.0$ Hz, 2H, Ar-H), 7.40–7.31 (m, 2H, Ar-H), 7.09 (s, 1H, -$C = C$–H), 7.04–7.00 (m, 2H, Ar-H); ^{13}C NMR (151 MHz, DMSO–d_6): δ 160.5, 159.8, 154.1, 146.1, 142.4, 137.4, 136.0, 131.5, 130.6, 130.0, 129.8, 129.3, 129.0, 128.5, 127.8, 124.0, 123.6, 116.8, 116.0, 115.6, 114.8; accurate mass (EI-MS) of $[M]^{+\bullet}$: Calcd. for $C_{21}H_{13}{}^{35}ClN_4O_5$ 436.05740; found 436.05723.

3.1.4. N-(4-(4-(2-(2,4-Dinitrophenyl)hydrazono)−4H-chromen-2-yl)phenyl)acetamide

(3d)

Dark-maroon crystalline solid; Yield: 70%; M.P. 233–235 °C; $R_f = 0.5$; UV–Vis λ_{max} (CH_3CN) = 231, 369 nm; λ_{em} (CH_3CN) = 412, 731 nm; FTIR (cm^{-1}): 3303 (N–H str.), 3112 (aromatic C–H str.), 1614 (s, $C = N$ str.), 1592 (m, aromatic $C = C$ str.), 1546 (C–NO_2 asym.), 1378 (C–NO_2 sym.), 1330 (C–N str.), 1273 (C–O str.), 1135 (C–NH str.), 762 (*p*-monosubstituted); ^{1}H NMR (600 MHz, DMSO–d_6): δ 11.54 (s, 1H, -$N = N$–H), 10.50 (bs, 1H, $NHCOCH_3$), 8.84 (d, $J = 6.0$ Hz, 1H, Ar-H), 8.43 (dd, $J = 12.0, 6.0$ Hz, 1H, Ar-H), 8.02 (d, $J = 12.0$ Hz, 1H, Ar-H), 7.80 (d, $J = 12.0$ Hz, 2H, Ar-H), 7.35 (dd, $J = 12.0, 6.0$ Hz, 1H, Ar-H), 7.35–7.10 (m, 3H, Ar-H), 7.07 (s, 1H, -$C = C$–H), 6.90 (d, $J = 12.0$ Hz, 2H, Ar-H), 2.15 (s, 3H, $COCH_3$); ^{13}C NMR (151 MHz, DMSO–d_6): δ 170.2, 160.7, 159.6, 154.0, 145.1.0, 141.1, 137.6, 136.0, 130.1, 129.8, 129.2, 129.0, 128.7, 128.0, 124.0, 123.1, 116.4, 115.0, 114.7, 25.2; accurate mass (EI-MS) of $[M]^{+\bullet}$: Calcd. for $C_{23}H_{17}N_5O_6$ 459.11788; found 459.11768.

3.1.5. 1-(2-(2,4-Dimethylphenyl)−4H-chromen-4-ylidene)−2-(2,4-dinitrophenyl)hydrazine

(3e)

Dark-orange powder; Yield: 75%; M.P. 177–179 °C; $R_f = 0.7$; UV–Vis λ_{max} (CH_3CN) = 213, 362 nm; λ_{em} (CH_3CN) = 420, 739 nm; FTIR (cm^{-1}): 3309 (N–H str.), 3087 (aromatic C–H str.), 1614 (s, $C = N$ str.), 1585 (m, aromatic $C = C$ str.), 1535 (C–NO_2 asym.), 1336 (C–NO_2 sym.), 1308 (C–N str.), 1279 (C–O str.), 1215 (C–Me str.), 762 (*o*, *p*-disubstituted); ^{1}H NMR (600 MHz, DMSO–d_6): δ 11.53 (s, 1H, -$N = N$–H), 8.83 (d, $J = 6.0$ Hz, 1H, Ar-H), 8.41 (dd, $J = 12.0, 6.0$ Hz, 1H, Ar-H), 8.02 (d, $J = 12.0$ Hz, 1H, Ar-H), 7.70 (dd, $J = 12.0, 6.0$ Hz, 1H, Ar-H), 7.64 (dd, $J = 12.0, 6.0$ Hz, 1H, Ar-H), 7.53 (d, $J = 12.0$ Hz, 1H, Ar-H), 7.24 (dd, $J = 12.0, 6.0$ Hz, 1H, Ar-H), 7.10 (d, $J = 6.0$ Hz, 1H, Ar-H), 7.02 (s, 1H, -$C = C$–H), 2.38 (s, 6H, Me); ^{13}C NMR (151 MHz, DMSO–d_6): δ 160.1, 159.0, 154.0, 143.8, 140.1, 137.0, 135.6, 131.0, 130.0, 129.3, 129.0, 128.4, 128.0, 123.5, 123.0, 116.5, 115.1, 114.7, 64.0, 21.6, 21.1; accurate mass (EI-MS) of $[M]^{+\bullet}$: Calcd. for $C_{23}H_{18}N_4O_5$ 430.12772; found 430.12750.

3.1.6. 4-(4-(4-(2-(2,4-Dinitrophenyl)hydrazono)4H-chromen-2-yl)phenyl)morpholine

(3 g)

Dark-red crystalline solid; Yield: 80%; M.P. 139–141 °C; $R_f = 0.8$; UV–Vis λ_{max} (CH_3CN) = 267, 374 nm; λ_{em} (CH_3CN) = 409, 724 nm; FTIR (cm^{-1}): 3312 (N–H str.), 3084 (aromatic C–H str.), 1610 (s, $C = N$ str.), 1591 (m, aromatic $C = C$ str.), 1508 (C–NO_2 asym.), 1420 (C–NO_2 sym.), 1306 (C–N str.), 1279 (C–O str.), 1224 (aromatic C–N str.), 763 (*p*-monosubstituted); ^{1}H NMR (600 MHz, DMSO–d_6): δ 11.52 (s, 1H, -$N = N$–H), 8.86 (d, $J = 6.0$ Hz, 1H, Ar-H), 8.44 (dd, $J = 12.0, 6.0$ Hz, 1H, Ar-H), 8.04 (d, $J = 12.0$ Hz, 1H, Ar-H), 7.98 (d, $J = 12.0$ Hz, 2H, Ar-H), 7.91 (d, $J = 12.0$ Hz, 2H, Ar-H), 7.04 (s, 1H, -$C = C$–H), 3.57 (m, 4H, –N (CH2)$_2$), 3.05 (m, 4H, -N(CH_2)$_2$);^{13}C NMR (151 MHz, DMSO–d_6): δ 161.0, 159.6, 157.5, 154.1, 145.7, 140.0, 139.1, 137.0, 131.3, 129.8, 128.9, 128.4, 128.2, 127.7, 123.5, 122.8, 116.7, 115.5, 114.5, 55.6, 30.7; accurate mass (EI-MS) of $[M]^{+\bullet}$: Calcd. for $C_{25}H_{21}N_5O_6$ 487.14918; found 487.14901.

3.1.7. 1-(2,4-Dinitrophenyl)−2-(2-(thiophen-3-yl)−4H-chromen-4-ylidene)hydrazine

(3i)

Dark orange-maroon powder; Yield: 69%; M.P. 124–126 °C; $R_f = 0.7$; UV–Vis λ_{max} (CH_3CN) = 217, 374 nm; λ_{em} (CH_3CN) = 390, 700 nm; FTIR (cm^{-1}): 3310 (N–H str.), 3094 (aromatic C–H str.), 1613 (s, $C = N$ str.), 1587 (m, aromatic $C = C$ str.), 1537 (C–NO_2 asym.), 1355 (C–NO_2 sym.), 1330 (C–N str.), 1278 (C–O str.), 1214 (C–Thiophene str.), 765 (*p*-monosubstituted); ^{1}H NMR (600 MHz, DMSO–d_6): δ 11.50 (s, 1H, -$N = N$–H), 8.83 (d, $J = 6.0$ Hz, 1H, Ar-H), 8.40 (dd, $J = 12.0, 6.0$ Hz, 1H, Ar-H), 8.03 (d, $J = 12.0$ Hz, 1H, Ar-H), 7.99–7.98 (m, 2H, Ar-H), 7.90 (dd, $J = 12.0, 6.0$ Hz, 1H, Ar-H), 7.60–7.50 (m, 2H, Ar-H),7.35–7.20 (m, 2H, Ar-H), 7.05 (s, 1H, -$C = C$–H); ^{13}C NMR (151 MHz, DMSO–d_6): δ 161.1, 159.2, 158.6, 153.0, 152.1, 143.2, 139.0, 136.1, 134.3, 130.4, 129.6, 128.8, 128.7, 127.3, 126.7,123.5, 118.0, 114.5, 106.0; accurate mass (EI-MS) of $[M]^{+\bullet}$: Calcd. for $C_{19}H_{12}N_4O_5S$ 408.05284; found 408.05260.

3.1.8. 3-(4-(2-(2,4-Dinitrophenyl)hydrazono)−4H-chromen-2-yl)−1-tosyl-1H-indole

(3j)

Dark maroon powder; Yield: 71%; M.P. 166–168 °C; $R_f = 0.6$; UV–Vis λ_{max} (CH_3CN) = 215, 264, 365 nm; λ_{em} (CH_3CN) = 415, 749 nm; FTIR (cm^{-1}): 3362 (N–H str.), 3102 (aromatic C–H str.), 1614 (s, $C = N$ str.), 1583 (m, aromatic $C = C$ str.), 1513 (C–NO_2 asym.), 1375 (C–NO_2 sym.), 1329 (C–N str.), 1250 (C–O str.), 1215 (C–Sulfonamide str.), 762 (*p*-monosubstituted); ^{1}H NMR (600 MHz, DMSO–d_6): δ 11.58 (s, 1H, -$N = N$–H), 8.87 (d, $J = 6.0$ Hz, 1H, Ar-H), 8.43 (dd, $J = 12.0, 6.0$ Hz, 1H, Ar-H), 8.04 (d, $J = 12.0$ Hz, 1H, Ar-H), 8.00–7.94 (m, 2H, Ar-H), 7.85–7.60 (m, 3H, Ar- H), 7.507.28 (m, 2H, Ar-H), 7.22 (d, $J = 12.0$ Hz, 2H, Ar-H), 7.10 (s, 1H, –$C = C$–H), 7.08–7.02 (m, 1H, Ar-H), 6.98 (d, $J = 12.0$ Hz, 2H, Ar-H), 6.40 (m, 1H, Ar-H), 2.30 (s, 3H, CH_3); ^{13}C NMR (151 MHz, DMSO-d_6): δ 162.0, 159.8, 153.8, 148.2, 147.0, 141.7, 139.0, 138.8, 135.8, 133.5, 131.7, 130.2, 129.8, 129.5, 129.0, 128.7, 128.2, 127.3, 126.0, 124.8, 124.0, 120.7, 120.1, 119.8, 118.5, 116.4, 115.9, 114.5, 111.5, 21.5; accurate mass (EI-MS) of $[M]^{+\bullet}$: Calcd. for $C_{30}H_{21}N_5O_7S$ 595.11617; found 595.11602.

3.1.9. 4-(4-(2-(2,4-Dinitrophenyl)hydrazono)−4H-chromen-2-yl)-N,N-dimethylaniline

(3l)

Dark maroon crystalline solid; Yield: 73%; M.P. 181–183 °C; $R_f = 0.6$; UV–Vis λ_{max} (CH_3CN) = 214, 379 nm; λ_{em} (CH_3CN) = 427, 750 nm; FTIR (cm^{-1}): 3032 (N–H str.), 3010 (aromatic C–H str.), 1614 (s, $C = N$ str.), 1584 (m, aromatic $C = C$ str.), 1508 (C–NO_2 asym.), 1390 (C–NO_2 sym.), 1361 (C–N str.), 1241 (C–O str.), 1232 (C–dimethylaniline str.), 759 (*p*-monosubstituted); ^{1}H NMR (600 MHz, DMSO–d_6): δ 11.51 (s, 1H, -$N = N$–H), 8.81 (d, $J = 6.0$ Hz, 1H, Ar-H), 8.40 (dd, $J = 12.0, 6.0$ Hz, 1H, Ar-H), 8.01 (d, $J = 12.0$ Hz, 1H, Ar-H), 7.96 (d, $J = 12.0$ Hz, 2H, Ar-H), 7.88 (d, $J = 12.0$ Hz, 2H, Ar-H), 7.01 (s, 1H, -$C = C$–H), 3.06 (s, 6H, –N (CH_3)$_2$);^{13}C NMR (151 MHz, DMSO–d_6): δ 160.2, 159.1, 158.0, 153.1, 145.1, 141.0, 138.0, 135.5, 130.0, 129.0, 128.5, 128.5, 128.2, 128.0, 123.1, 122.3, 116.0, 115.1, 114.4, 30.1; accurate mass (EI-MS) of $[M]^{+\bullet}$: Calcd. for $C_{23}H_{19}N_5O_5$ 445.13862; found 445.13850.

3.1.10. 1-(2,4-Dinitrophenyl)−2-(2-(4-ethoxyphenyl)−4H-chromen-4-ylidene)hydrazine

(3 m)

Dark-red powder; Yield: 89%; M.P. 170–172 °C; $R_f = 0.9$; UV–Vis λ_{max} (CH_3CN) = 273, 414 nm; λ_{em} (CH_3CN) = 429, 730 nm; FTIR (cm^{-1}): 3302 (N–H str.), 3112 (aromatic C–H str.), 1614 (s, $C = N$ str.), 1598 (m, aromatic $C = C$ str.), 1515 (C–NO_2 asym.), 1329 (C–NO_2 sym.), 1306 (C–N str.), 1272 (C–O str.), 1219 (C–OCH_2CH_3 str.), 761 (*p*-monosubstituted); ^{1}H NMR (600 MHz, DMSO–d_6): δ 11.55 (s, 1H, -$N = N$–H), 8.85 (d, $J = 6.0$ Hz, 1H, Ar-H), 8.42 (dd, $J = 12.0, 6.0$ Hz, 1H, Ar-H), 8.02 (d, $J = 12.0$ Hz, 1H, Ar-H), 7.68 (d, $J = 12.0$ Hz, 1H, Ar-H), 7.62 (d, $J = 12.0$ Hz, 1H, Ar-H), 7.30–7.21 (m, 2H, Ar-H), 7.06 (s, 1H, -$C = C$–H), 7.03–7.01 (m, 2H, Ar-H), 6.95 (d, $J = 12.0$ Hz, 2H, Ar-H), 4.11–4.04 (m, 2H, -O$\underline{CH_2}CH_3$), 1.37–1.33

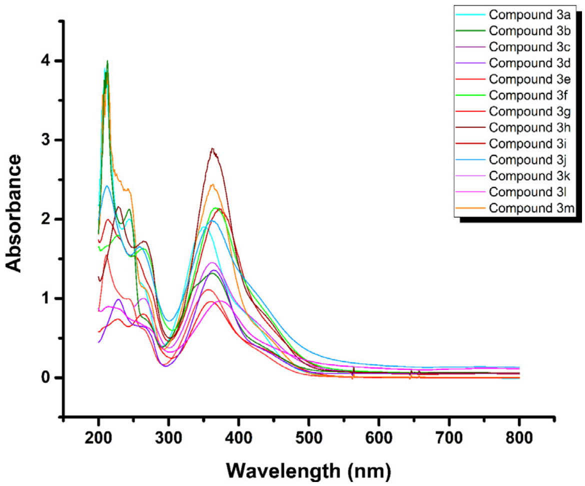

Fig. 2. A comparative absorption spectra of synthesized hydrazones (**3a-3 m**).

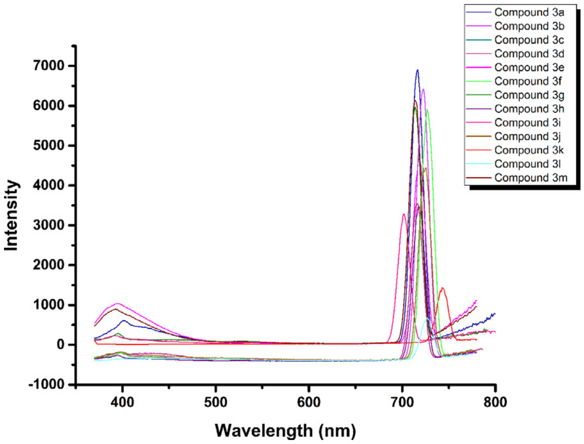

Fig. 3. A comparative fluorescence spectra of synthesized hydrazones (**3a-3 m**).

(m, 2H, $\text{-OCH}_2\underline{\text{CH}_3}$); ^{13}C NMR (151 MHz, DMSO–d_6): δ 160.2, 159.7, 153.9, 144.0, 140.0, 137.5, 136.5, 130.5, 130.0, 129.5, 129.4, 128.9, 128.2, 123.7, 123.4, 116.7, 115.2, 115.1, 114.8, 64.0, 15.0 (two aromatic carbons are isochronous); accurate mass (EI-MS) of $[M]^{+\bullet}$: Calcd. for $C_{23}H_{18}N_4O_6$ 446.12263; found 446.12244.

3.2. Electronic absorption study

The UV–Vis absorption of hydrazones is recorded in the CH_3CN solution. It has been generally assumed that the peaks in 300–390 nm range are involved $\pi\rightarrow\pi^*$ transitions associated with azomethine ($C = N$) groups and phenyl rings whereas the peaks in 211–410 nm range might be allotted to $\pi\rightarrow\pi^*$ and $n\rightarrow\pi^*$ transitions of the aryl rings and $C = N$ bond etc. Moreover, in these hydrazones, a peak observed at 432 nm was perturbed in their 2,4-DNPH derivatives, which supports the condensation of the 2,4-DNPH with substituted flavones. The maximum absorption bands stretching from 340 to 400 nm are assigned to the intramolecular charge transfer band of the azomethine $C = N$ group. Moreover, λ_{max} of Schiff bases in UV absorption studies is influenced by the inductive and resonance effect of substituents. The introduction of an electron-withdrawing or electron-donating substituent leads to a general trend of λ_{max} hypsochromic shift. The absorption maxima (λ_{max}) for the compounds **(3a-3 m)** showed some difference in absorption wavelength due to the presence of various substituents at the *p*-position of the hydrazone derivatives. Surprisingly, the EDG groups such as *p*-OCH_3 and *p*-CH_3, *etc.* at the 4′-position of the ring B of chromone derivatives shifts λ_{max} towards longer wavelengths, resulting in a bathochromic (red) shift, whereas the EWG groups such as *p*-Cl and *p*-F, *etc.* results in the hypsochromic (blue) shift. The absorption peaks are affected substantially by the aromatic moieties on the terminal phenyl moiety (Fig. 2).

3.3. Electronic emission study

Attaching several functional moieties to hydrazones at 4′-position may not only open numerous routes for the advancement in enhanced supramolecular structures, but also they may affect the emission properties of the parent analogs. Owing to their potent functions in electroluminescent displays, fluorescent materials and chemical sensors, have become a significant concern. According to the structural evaluation, the compound has a larger *p*-conjugated phenyl system capable of acquiring potent luminescence and effective energy transfer. The emission spectra of hydrazones (**3a-3 m)** were measured in CH_3CN solution at room temperature with an excitation wavelength of 315 nm for the synthesized derivatives. Substituted flavone analogs have a lot of potential as fluorescence probes for bio-labeling in an aqueous medium [16]. The synthesized compounds, when irradiated with UV radiation, were observed to have fluorescence properties in the blue portion of the visible region. However, emission intensities showed that the alkyl groups have a startling effect on the emission strength of flavone hydrazone derivatives. The alkyl substituents at the ring B could likely have some effect on the physicochemical properties due to its electron-donating nature and if we substitute the 2-aryl group of hydrazones with any heterocyclic moiety having extended conjugation, the product exhibited better fluorescence properties. From the fluorescence spectra (Fig. 3)of the envision compounds, it can be assumed that the insertion of EDG at ring B considerably influences the emission intensity without affecting any blue or redshift in the emission wavelength, and EWG offers a reverse effect. 'In the 4th position of the aryl compounds, various functionalities with various electron-releasing and -accepting properties have been added to further investigate, explore and alter the luminescent features of flavone hydrazones. The various substituents on flavone hydrazone scaffold generate a wider range of 394–769 nm for their emission spectra (Table 1).

Fig. 3.

3.4. FTIR study

The structures of the synthesized hydrazones (**3a-3 m**) were confirmed by the absorption peaks found at their corresponding frequencies. Peaks indicating absorption for *v*(N–H), *v*(*C*=*C*) and *v*(C–O) in ranges 3390–3300 cm^{-1}, 1560–1670 cm^{-1} and 1120–1280 cm^{-1} individually established the presence of imino linkage in the hydrazones. Another peak in the region 1601–1680 cm^{-1} showed the presence of *v*(*C*=*N*) linkage in the hydrazones. The aim of the vibrational analysis is to decide which of the vibrational modes in the molecule gives rise to each of the observed bands at specific wavenumbers in the FTIR spectra. The functional groups present in the molecule were identified and a satisfactory vibrational band assignment has been made for the fundamental modes of vibration by observing the position, shape and intensity of the bands. The spectra of the synthesized compounds (**3a-3 m**) also show several weak bands for the aliphatic and aromatic C–H and C–O stretching vibration frequencies at the region of 2840–3070 cm^{-1} and 1378–1450 cm^{-1}, respectively. The existence of a strong band at 1340–1530 cm^{-1} is consolidating the presence of the NO_2 functional group in the flavone hydrazones scaffold (Figure S5 in SI). The NH stretching vibration gives rise to a weak

Table 1
Emission and absorption data of all the targeted flavones hydrazones **(3a-3 m)**.

Compound No.	Solvent	$\lambda_{excitation}$ (nm)	$\lambda_{emission}$ (nm)	$\lambda_{absorption}$ (nm)	Transitions	Stoke Shift λ (nm)
3a.	Acetonitrile	368	378, 717	290, 358	$\pi \rightarrow \pi*(C=N), \pi \rightarrow \pi* \& n \rightarrow \pi*$ (aromatic rings)	359
3b.	Acetonitrile	378	421, 744	212, 368	$\pi \rightarrow \pi*(C=N), \pi \rightarrow \pi* \& n \rightarrow \pi*$ (aromatic rings)	376
3c.	Acetonitrile	375	417, 734	214, 365	$\pi \rightarrow \pi*(C=N), \pi \rightarrow \pi* \& n \rightarrow \pi*$ (aromatic rings)	369
3d	Acetonitrile	379	412, 731	231, 369	$\pi \rightarrow \pi*(C=N), \pi \rightarrow \pi* \& n \rightarrow \pi*$ (aromatic rings)	362
3e.	Acetonitrile	372	420, 739	213, 362	$\pi \rightarrow \pi*(C=N), \pi \rightarrow \pi* \& n \rightarrow \pi*$ (aromatic rings)	377
3f.	Acetonitrile	385	428, 752	229, 375	$\pi \rightarrow \pi*(C=N), \pi \rightarrow \pi* \& n \rightarrow \pi*$ (aromatic rings)	377
3 g.	Acetonitrile	384	409, 724	267, 374	$\pi \rightarrow \pi*(C=N), \pi \rightarrow \pi* \& n \rightarrow \pi*$ (aromatic rings)	350
3 h.	Acetonitrile	375	415, 738	231, 365	$\pi \rightarrow \pi*(C=N), \pi \rightarrow \pi* \& n \rightarrow \pi*$ (aromatic rings)	373
3i.	Acetonitrile	384	390, 700	217, 374	$\pi \rightarrow \pi*(C=N), \pi \rightarrow \pi* \& n \rightarrow \pi*$ (aromatic rings)	326
3j.	Acetonitrile	375	415, 749	215, 264, 365	$\pi \rightarrow \pi*(C=N), \pi \rightarrow \pi* \& n \rightarrow \pi*$ (aromatic rings)	384
3k.	Acetonitrile	383	410, 740	275, 373	$\pi \rightarrow \pi*(C=N), \pi \rightarrow \pi* \& n \rightarrow \pi*$ (aromatic rings)	367
3l	Acetonitrile	389	427, 750	214, 379	$\pi \rightarrow \pi*(C=N), \pi \rightarrow \pi* \& n \rightarrow \pi*$ (aromatic rings)	371
3 m.	Acetonitrile	407	429, 730	273, 396	$\pi \rightarrow \pi*(C=N), \pi \rightarrow \pi* \& n \rightarrow \pi*$ (aromatic rings)	316

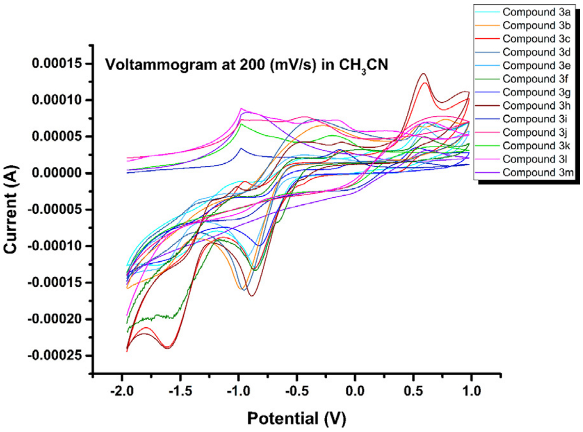

Fig. 4. A comparative cyclic voltammograms of synthesized hydrazones at 200 mV/s scan rate **(3a-3 m)**.

band at 3500–3300 cm^{-1}. A stronger band at 750–700 cm^{-1} in secondary aliphatic amines is due to NH stretching. Secondary aromatic amines have a CNH bending absorption near 1510 cm^{-1} near the 1500 cm^{-1} aromatic band.

3.5. ^{1}H and ^{13}C NMR spectroscopy

NMR calculations are now attainable and accurate enough to be useful in exploring the relationship between chemical shift and molecular structure. The experimental ^{1}H NMR spectrum of the product (**3 m**) in DMSO–d_6 is given in SI Figure S6. The ^{1}H NMR chemical shifts (δ/ppm) of all the targeted compounds **(3a-3 m)** are assigned in the Result and discussion section.

3.6. Cyclic voltammetric analysis

The electrochemical properties of flavone hydrazones **(3a-3 m)** were investigated employing the CV method. The analysis was recorded in the potential range of –2.0 to +1.0 V at 25 °C with the scan rate of 200, 100 and 40 mV/s. The CV was initially run for CH_3CN as a blank solution within the desired potential range of –2.0 to +1.0 V. CV response for blank has ensured the media purity as no peak was detected in both reverse and forward scan.

The analysis of hydrazone compounds' redox properties supported in assessing their electron-transfer potential. The electrochemical properties of the flavone hydrazones were examined by CV on a 0.1 mM solution of the hydrazone at a Pt electrode in CH_3CN having 0.1 M TBAB as supporting electrolyte at a 200 mVs^{-1} scan rate.

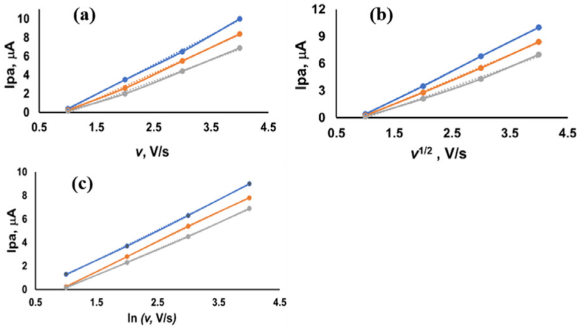

Fig. 5. The relation between I_{pa} for 200, 100 and 40 mVs^{-1} of Compound 3a with **(a)** scan rate (υ); **(b)** square root of $\upsilon(\upsilon^{1/2})$; **(c)** lnυ. In these figures, blue color indicates 200 mVs^{-1}, brown color indicates 100 mVs^{-1} and gray color indicates 40 mVs^{-1}.

Fig. 4 indicates three quasi-reversible oxidation peaks for the flavone hydrazones, and the presence of one or two cathodic peaks indicated the number of electrons transferred is more than two electrons. Ever since, the peak has been followed by two more physically adsorbed, compressed films, each of which corresponds to a physically adsorbed process at extremely negative potential.

Moreover, peak potentials ($E_{pc,}$ E_{pa}) and their consequent peak currents ($I_{pc,}$ I_{pa}) values were estimated from Fig. 5 by certain factors, for example, peak potential difference ($\mathbf{\Delta E = E_{pa} - E_{pc}}$) and the anodic-cathodic currents ratio (I_{pa}: I_{pc}) were determined and mentioned in Table 2. The various factors in Table 2 proved that the redox outcomes of the hydrazones correspond to quasi-reversible procedures where the difference in potential values are greater than 0.3 V and the I_{pa}: I_{pc} in the majority cases is lesser than 1. Likewise, the $E_{1/2}$ for quasi-reversible and reversible reactions determined by applying subsequent expression and given in Table 2:

$$\mathbf{E_{1/2} = E_{pa} - DE/2}$$

The oxidation peaks potential and the half peak potential move towards more positive potentials upon linkage, representing superficial hydrazones oxidation due to the presence of electron-donating moiety with an electron-withdrawing moiety which decreases the electron density on the ring making -NH moiety less disposed to oxidation.

3.7. Effect of scan rate

Scan rate is a factor that influences the electrooxidation of several molecules. Using cyclic voltammetry, the impact of scan rate on electrooxidation of hydrazone was studied from –2.0 to +1.0 Vs^{-1} (Figure S4 in SI). The peak potential and current for flavone

Table 2
Peak currents, Peak potentials, and potential peak difference of the flavone hydrazones in CH_3CN of 0.1 mM concentration at scan rate 200 mV/s.

Compound No.	E_{pa}s[a] (V)	E_{pc}s[b] (V)	ΔE[c] (V)	I_{pa}[d]: I_{pc} [e] (μA)	E½ (V)
3a.	−0.50, 0.25, 0.75	−0.80	0.3	20, 25, 70 130	−0.65
3b.	−0.25, 0.50, 0.75	−0.85	0.6	33, 30, 35 130	−0.55
3c.	−0.25, 0.50, 0.75	−0.85, −1.5	0.6	33, 30, 35 130	−0.55
3d	−0.20, –, 0.60	−0.80, −1.5	0.6	25,–, 100 125, 240	−0.50
3e.	−0.25, –, 0.60	−0.85, −1.5	0.6	40, –,30 130	−0.50
3f.	−0.4, −0.1, 0.6	−0.75, −1.3	0.35	30, 35, 80 210, 120	−0.57
3 g.	−0.4, 0.3, 0.75	−0.75, −1.5	0.35	20, 10, 50 150, 210	−0.57
3 h.	−0.5, −0.2, 0.6	−0.85, −1.6	0.35	30, 20, 10 150, 200	−0.67
3i.	−0.5, −0.2, 0.7	−0.80, −1.5	0.35	20, 30, 90 100, 180	−0.67
3j.	−0.5, –, 0.75	−0.85	0.35	40, 50 150	−0.67
3k.	−0.5, 0.5, 0.7	−0.80, −1.5	0.3	30, 50, 20 150	−0.65
3l	−0.5, 0.25, 0.5	−0.80, −1.4	0.3	25, 20, 10 90, 70	−0.65
3 m.	−0.4, 0.25, 0.75	−0.75, −1.5	0.35	30, 15, 10 90, 110	−0.57

[a] E_{pa} = Anodic Peak Potential;.
[b] E_{pc} = Cathodic Peak Potential;.
[c] ΔE = Difference of E_{pa} & E_{pc};.
[d] I_{pa} = Anodic Peak Current;.
[e] I_{pc} = Cathodic Peak Current.

hydrazone electrooxidation were determined using cyclic voltammograms. The analysis of the reliance of I_p on $v^{1/2}$ and the analysis of the reliance of $\ln I_p$ on $\ln v$ are two conventional methods for determining the reversibility of reactions and determining whether they are diffusion-controlled or adsorption-controlled. The impact of the scan level on the electrooxidation of 0.1 mM solution of hydrazones was studied in the range 200, 100 and 40 mVs^{-1} as displayed in Figure S4 in SI.

It can be noticed from Fig. 5 that, the oxidation peaks' potential moved more toward positive values as the level of scan increased, while the reduction peaks potential moved more toward negative numbers, and all peaks' currents shifted toward higher numbers. The quasi-reversible state is ensured by the shift in the redox peaks as the scan rate is changed. The compounds with electron-withdrawing substituents made the electrooxidation difficult while the compound with electron-donating substituents made the electrooxidation easy. This is very much in agreement with the reported work on similar compounds.

The consecutive oxidation signals are ascribed to the 'chromen-4-ylidene' unit and the substituent attached. The reduction signals are due to dinitrophenyl hydrazine linkage. More specifically due to the dinitrophenyl unit. The dinitrobenzene typically gives its quasi-reversible signatures in the range of −0.5 to −1.5 V. Quite obviously, the environment affects the peak potential positions. The signal appearing around +0.5 V appears to be due to the hydrazone unit. The results also demonstrate that electrochemically the hydrazone derivatives are a multi-electron transfer process. This indicates their rich electroactivity with more than one electroactive center and thus makes them very interesting compounds to be investigated further for their electrochemical character.

As shown in Figure (5a), the three current oxidation peak and a scan rate of compound **3a** is linearly related and explained by the given equations:

$$\text{For } 1^{st} \text{ oxidationpeak}: \ I_{pa} = \{3.18\, \upsilon(Vs^{-1})\}\, \mu A - 2.85\, \mu A;\ R^2 = 0.9989$$
$$\text{For } 2^{nd} \text{ oxidationpeak}: \ I_{pa} = \{2.735\, \upsilon(Vs^{-1})\}\, \mu A - 2.65\, \mu A;\ R^2 = 0.9976$$
$$\text{For } 3^{rd} \text{ oxidationpeak}: \ I_{pa} = \{2.262\, \upsilon(Vs^{-1})\}\, \mu A - 2.29\, \mu A;\ R^2 = 0.9956$$

Fig. 6a illustrates that as the rate of scan is increased, the anodic peak current of the three anodic peaks increases, implying that the reactions are regulated by diffusion. Using following equation, the no. of transferred electrons throughout the compound's oxidation reaction was estimated from the linear relationship slope between v and I_p:

$$Ip = \frac{nFQv}{4RT}$$

where,

Q = The quantity of charge obtained by integrating of the area of cyclic voltammetric peak; F = Faraday's constant (96,487 $Cmol^{-1}$); R = The universal gas constant (8.3143 $Jmol^{-1}K^{-1}$); T = Kelvin temperature (298 K).

The total no. of transferred electrons (n) was 3.3 (≈3).

According to the HOMO, LUMO and the strength of the density of electronic charge on the hydrazone moiety, the nitrogen atoms that have a greater electron density than C and O atoms correspond to the oxidizable moiety.

In the scan rate range from −2.0 to 0.1 Vs^{-1}, peak current (I_p) of hydrazone electrooxidation depends linearly on the $\upsilon^{1/2}$ (Fig. 5b) and is demonstrated by the equations:

$$\text{For } 1^{st} \text{ oxidationpeak}: \ I_{pa} = \{3.210\, \upsilon^{1/2}(Vs^{-1})^{1/2}\}\, \mu A - -2.85\, \mu A;\ R^2 = 0.9999$$
$$\text{For } 2^{nd} \text{ oxidationpeak}: \ I_{pa} = \{2.715\, \upsilon^{1/2}(Vs^{-1})^{1/2}\}\, \mu A - -2.55\, \mu A;\ R^2 = 0.9992$$
$$\text{For } 3^{rd} \text{ oxidationpeak}: \ I_{pa} = \{2.272\, \upsilon^{1/2}(Vs^{-1})^{1/2}\}\, \mu A - -2.295\, \mu A;\ R^2 = 0.9946$$

The existence of a coefficient value of the linear relation of I_p of the compound **3a** oxidation peaks with $\upsilon^{1/2}$ shows that a chemical reaction has occurred on the electrode surface.

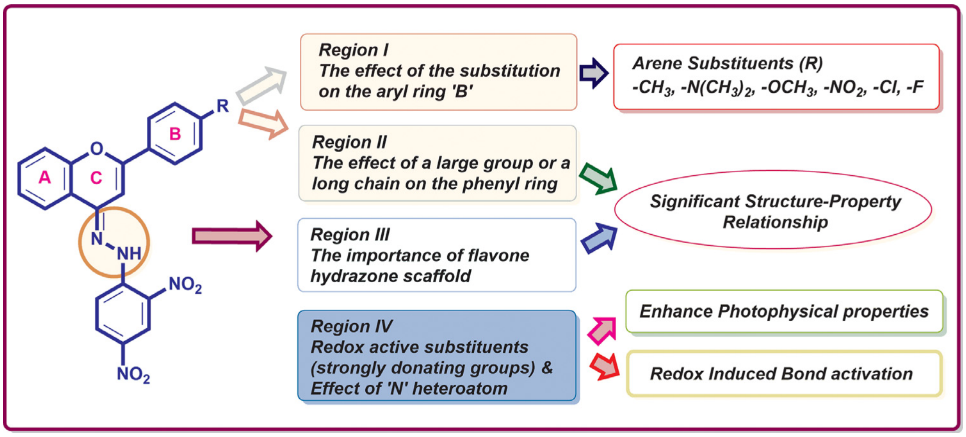

Fig. 6. Structure-property relationship of synthesized flavone hydrazones (**3a-3 m**).

Moreover, the graph of $\ln I_p$ with $\ln \upsilon$ Figure (5c) is linear with curves that are far from the value of 0.5 (for pure diffusion) but near to 1, indicating that electrode reaction is regulated by adsorption as well as diffusion. This relationship can be explained using the following equations:

$$\text{For } 1^{\text{st}} \text{ oxidationpeak}: \ \ln I_{pa} = \{2.57 \ \ln \upsilon (Vs^{-1})\} \, A - -1.35 \, A; \ R^2 = 0.9993$$
$$\text{For } 2^{\text{nd}} \text{ oxidationpeak}: \ \ln I_{pa} = \{2.525 \ \ln \upsilon (Vs^{-1})\} \, A - -2.25 \, A; \ R^2 = 0.9997$$
$$\text{For } 3^{\text{rd}} \text{ oxidationpeak}: \ \ln I_{pa} = \{2.233 \ \ln \upsilon (Vs^{-1})\} \, A - -2.115 \, A; \ R^2 = 0.9992$$

3.8. Structure-property relationship

The aryl substituents on the terminal benzene moiety had a major impact on absorption behavior. Compared with the aryl-substituted compounds, EWGs such as the –Cl, $-NO_2$, –F create a noticeable hypsochromic and EDGs like ($-N(CH_3)_2$, $-OCH_3$, $-NHCOCH_3$, $(-OCH_3)_2$) affect bathochromic (red) shifts of the $\pi - \pi *$ band, respectively. This study can explain by the expanded systems of conjugated π-electrons of hydrazones *via* the non-bonding electron pairs of the 'N' atoms. A broad absorption peak for hydrazone derivatives **(3a-3 m)** is attributable to the $\pi - \pi^*$ transitions of a conjugate backbone with absorption λ_{max} in the range of 290–414 nm. Furthermore, owing to the existence of a related flavone hydrazone nucleus for all the derivatives, the spectral curves are identical in the electronic ultraviolet absorption spectra. It is remarkable, that the variation in wavelength and absorption strength is ascribe merely to the impact of the *p*-alkyl phenyl moieties at the *p*-position of the 2-phenylchromone nucleus.

The fluorescence properties of compounds (**3a-3 m)** in CH_3CN solution have been examined and figure S2 in SI presents the emission spectral data. Similarly, Table 1 shows the emission levels. Various analogs bearing substituents with variable electronegativity demonstrate variable fluorescence properties at ambient temperature in the solution state. However, when the substituents are altered, the typical emission bands of these synthesized derivatives may be expected from 378 to 752 nm. The two bands are noticed in the emission spectra of all the synthesized compounds **(3a-3 m)**. For flavone hydrazones, their fluorescence spectra exhibit two bands, a lower intensity band in the range of 378 nm and another with high intensity in the range of 752 nm, when being excited at around 315 nm. Because of the various functionalities at the flavone scaffold, their emission bands display modifications. Most of them not only display fluorescence characteristics with maximum emission but also alter the maximum emission bands from 378 to 752 nm due to the different substituents. The emission spectra of the hydrazones **3a-3 m** were then analyzed at their corresponding excitation wavelengths. Based on the nature of their λ_{em} in the visible spectrum blue region, these derivatives (**3a-3 m**) also exhibit blue fluorescence. Blue fluorescence of certain molecules is thought to be due to the flavone motif and different substitution pattern. Aromatic moieties that present at the 4′-position of flavone structure form the conjugated $\pi-$backbone and are mostly accountable for photon absorption. Consequently, the substitution of aryl and alkyl substituents at *p*-position can be presumed to have some influence on physicochemical properties. These findings demonstrate that changing the alkyl group has a significant impact on emission strength without causing a drastic change in blue- or red-shift in λ_{em}, and the substitution of EDGs for the conjugated backbone of these molecules can be used to shift emission intensity. As a result, it is expected that the emission intensity can be modified by changing the flavone hydrazone ring substituents, which will be extremely valuable for regulating the fluorescence and optoelectronic features of OLEDs based on related luminescence molecules.

The electrochemical properties of the hydrazones **(3a-3 m)** solutions in acetonitrile have been studied by CV. These derivatives are known to be quasi-reversible and are electrochemically stable. The same values of cathodic and anodic peaks were detected for every molecule for three times repeated cycles at various scan rates 200, 100 and 40 mVs^{-1}. It was recognized that the position of different functional groups on the hydrazone scaffold can affect the redox behavior and current. In the presence of various substituents on flavone scaffold, **3a-3 m** at different scan rates show no noticeable difference in the cathodic/anodic peak position; however, raising the scan rate resulted in an increase in the current magnitude, suggesting that the electrochemical redox process is reversible. The oxidation peak potential of all the synthesized compounds moves to a more positive value. The presence of EDGs ($-CH_3$, $-N(CH_3)_2$, $-OCH_3$, $-NHCOCH_3$, *etc.*) at *p*-position of ring B of flavone hydrazone scaffold increases the redox behavior of the structural motif whereas the electron-withdrawing groups ($-NO_2$, -Cl, -F, *etc.*) at *p*-position of ring B decreases the redox behavior of the compounds. Furthermore, the replacement of aryl ring B with other heterocyclic rings such as thiophene, morpholine, sulfonamide-like moiety also displayed exceptional redox behavior. Apart from that, all other synthetic flavone hydrazones demonstrated moderate to excellent oxidation–reduction behavior. Changes in the values of $E_{1/2}$ are ascribed to the position of the $-NO_2$ group of 2,4-DNPH. Overall, the results presented herein show that nature and substitution patterns at rings B and C increase the redox potential of these molecules, and thus are accountable to control it. Since all the proposed structures have a common substituted flavone hydrazone skeleton in their scaffolds. Furthermore, these findings explain that the position, nature and no. of substituents on aryl ring significantly affect the physicochemical and electrochemical properties of these analogs **(3a-3 m)**. Detailed structure-property relationship is depicted in Fig. 6.

3.9. Density functional theory (DFT) study

***Frontier Molecular Orbitals Analysis**:* The HOMO orbital denotes the ability to donate an electron whereas LUMO designates the capability to accept the electron. Various functional groups of hydrazone derivatives **(3a-3j)** have the ability to change the positions of HOMO-LUMO energy gap, which markedly influences the oxidation and reduction patterns [45]. The highest reduction potential and most negative E_{LUMO} values designate the ease of reduction for a compound [46]. A more negative E_{LUMO} value indicates the favorability for the addition of electrons due to the lowering of energies of the orbitals. The compounds **3a** and **3 h** have shown the highest reduction potential and most negative E_{LUMO} values in comparison to others, which correspond to the easiest reduction (Table 3). A similar trend was observed from the experimental reduction potentials of compounds **(3a-3j)**. In the same way, less values of E_{HOMO} designates the ease of oxidation for a compound. The oxidation potentials measured from electrochemical studies were compared to the E_{HOMO} values obtained from DFT analysis [47]. Compound **3 g** has shown the least negative E_{HOMO} value among others corresponding to ease of oxidation whereas the oxidation potential of compound **3 g** from experimental studies has depicted the same (shown in Table 3).

The graphical representation of FMOs of representative compounds **(3a-3j)** in SI **(**Figure S7). The HOMO orbitals tend to be localized on the hydrazone core structure whereas the LUMO orbitals are spread over the *di*-nitrobenzene moiety (having EW atoms N and O). The E_{LUMO}-E_{HOMO} gaps for compounds **(3a-3j)** were in accordance with the band gaps analyzed from electrochemical studies *i.e.*, $\Delta E_p = E_{pa}$-E_{pc} [48] of the compounds shown in Table 3.

Chemical Reactivity Parameters: The chemical reactivity of a compound lays down its ability to be stabilized by attracting the charge from the environment [49]. The stability, electrical and chemical reactivity parameters of the analogs can be calculated using the energy gap between HOMO-LUMO orbitals [50]. By variating the energy band gap by substituting different functional groups within the hydrazone structures can be utilized in the modification of chemical reactivity patterns of the compounds. Chemical reactivity parameters *i.e.*, electronegativity (x) chemical hardness (η) and chemical potential (μ) and electrophilicity index (ω) were calculated following the literature [50]. Whereas, IP (-E_{HOMO}) corresponds to ionization potential and EA (-E_{LUMO}) is the electron affinity. These reactivity parameters were calculated for the compounds **(3a-3j)** and summarized in Table 4.

The chemical potential values of synthesized analogs indicated the energy absorbed or released due to oxidation and reduction processes for the compounds **(3a-3j)**. High negative potential values correspond to high reduction potential as compound **3a** has shown the high negative value and *vice versa*. But electrode potential is the sum of chemical potential and nonelectrical potential hence little fluctuation was observed which may be due to different functional groups variating the redox properties [52] (Table 3). A small energy gap indicates a soft and reactive compound, and on the other hand, a wide energy gap suggests a strong and slow-reacting molecule [53]. Compound **3 g** has the highest softness characteristics tends to be the most reactive one may be ascribed to the heterocyclic ring in the structure. Compounds **3a, 3c, 3 h**, and **3i** have shown a high value of global hardness tend to be stable and less reactive as given in Table 4. Moreover, analogs were found to have more charge transferability and most of the analogs are more reactive. The chemical reactivity characteristics determined that these molecules ascribed to have good redox properties.

Table 3
B3LYP calculated values of E_{LUMO}, E_{HOMO}, E_{HOMO}-E_{LUMO} gap (ΔE), oxidation potential (E_{pa}), reduction potential (E_{pc}), E_{pa}-E_{pc} gap (ΔE_p) of compounds **(3a-3j)**.

Compounds	E_{LUMO} (Hartee)	E_{HOMO} (Hartee)	E_{LUMO}-E_{HOMO} gap ΔE (Hartee)	Oxidation Potential (E_{pa}) mV	Reduction Potential (E_{pc}) mV	E_{pa}-E_{pc} gap ΔE_p (mV)
3a.	−0.11505	−0.21636	0.10131	−500	−800	300
3b.	−0.10587	−0.20511	0.09924	−250	−850	600
3c.	−0.10963	−0.20964	0.10003	−250	−850	600
3d	−0.10961	−0.20698	0.09737	−200	−800	600
3e.	−0.10896	−0.20779	0.09883	−250	−850	600
3f.	−0.10877	−0.20823	0.09946	−400	−750	350
3 g.	−0.10740	−0.19757	0.09017	−400	−750	350
3 h.	−0.11274	−0.21357	0.10083	−500	−850	350
3i.	−0.11214	−0.21301	0.10087	−300	−800	500
3j.	−0.10724	−0.20643	0.09919	−350	−850	500

Table 4
The DFT-B3LYP calculated chemical reactivity parameters of compounds **(3a-3j)**.

Compounds	Electron Affinity (EA)	Ionization Potential (IP)	Electro-negativity (x)	Electro philicity (ω)	Chemical Potential (µ)	Global Hardness (η)	Global Softness (σ)
3a.	0.11505	0.21636	0.16571	0.28052	−0.16858	0.05066	9.87069
3b.	0.10587	0.20511	0.15549	0.22588	−0.14972	0.04962	10.0766
3c.	0.10963	0.20964	0.15964	0.20389	−0.1428	0.05001	9.99900
3d	0.10961	0.20698	0.15829	0.21305	−0.14403	0.04869	10.2701
3e.	0.10896	0.20779	0.15838	0.22109	−0.14782	0.04942	10.1184
3f.	0.10877	0.20823	0.15850	0.23328	−0.15232	0.04973	10.0543
3 g.	0.10740	0.19757	0.15249	0.26005	−0.15313	0.04509	11.0902
3 h.	0.11274	0.21357	0.16316	0.21752	−0.14810	0.05042	9.91768
3i.	0.11214	0.21301	0.16258	0.26203	−0.16258	0.05044	9.91375
3j.	0.10724	0.20643	0.15684	0.24798	−0.15684	0.04959	10.0816

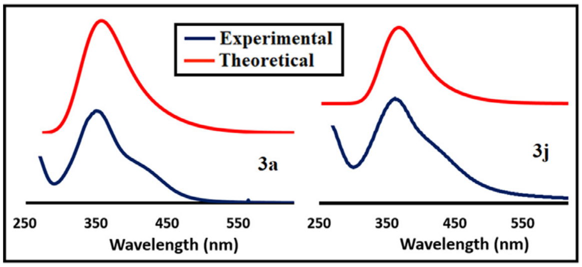

Fig. 7. Experimental and DFT-B3LYP/321 g calculated UV-Visible spectra of representative compounds **(3a and 3j)**.

Mullikens Atomic Charges Analysis: Mullikens atomic charges of represented compounds **(3a-3j)** calculated using DFT-B3LYP/3–21 G. Figure S8 in SI depicts Mulliken charge distribution on optimized compounds **(3a-3j),** denoted by a color transition on the atoms with a color scheme and scale (green for positive charge and red for negative charge). These charges have a very important role in the quantum chemical approach and affect the electronic structure and in turn influence redox patterns and also the reactivity for biological targets [54]. The existence of strongly electronegative atoms such as O, Cl, F, and N was revealed by the calculated values of atomic charges, indicating that positive charge is distributed on carbon atoms and on all forms of hydrogen atoms.

UV-Visible Analysis: UV-Visible spectra of representative compounds **3a** and **3j** were calculated by TD-DFT-B3LYP/321 g that explained the electronic absorption patterns in the compounds. Spectra of compounds **3a** and **3j** are given in Fig. 7 in comparison to their experimental UV–Vis spectra. Experimental and DFT calculated spectra for representative compounds were in good agreement to each other as depicted in Fig. 7.

Both these compounds have shown an intense absorption peak in the region 300–450 nm. involve $\pi\rightarrow\pi*$ and n$\rightarrow\pi*$ transitions of the aryl rings and $C = N$ bond *etc.* Moreover, broadening above 400 nm in spectra of these compounds is indicative of condensation of the 2,4-DNPH with substituted flavones as discussed in the experimental absorption analysis discussion. Slight peak shifting in absorption spectra is ascribed to substitutions on the terminal phenyl moiety. The compound **3j** having a *p*-CH_3 group at the 4′-position of the ring B of chromone derivatives shows a bathochromic (red) shift, whereas compound **3a** having group *p*-Cl results in the hypsochromic (blue) shift in accordance with the experimental results.

Vibrational Analysis: The vibrational frequencies, the nature of vibrational modes, and the potential energy distributions (PED) of the representative compounds **3a** and **3j** of flavone hydrazones are presented in Table 5 in comparison with the experimental results. Then, a detailed vibrational study based on PED [55] was performed employing the VEDA 4 program [51] based on the results of the B3LYP level [55a, b]. This reveals a good correspondence between theory and experiment in main spectral features. For a visual comparison, the recorded and calculated FT-IR spectra for compounds **3a** and **3j** are presented in Figs. 8a and 8b. The compound **3a** with 44 atoms denotes (3N-6) *i.e.,* 126 vibrational modes in the range 20–4000 cm^{-1} among which 43 stretching modes, 42 bending modes and 36 are torsional modes. Whereas for compound **3j** with 64 atoms ascribes (3N-6) *i.e.,* 186 vibrational modes among which 63 stretching, 62 bending, 61 torsional and 60 are C–H modes. Comparison of theoretical results with experimental data reveals a good correlation ($R^2 > 0.9$) in obtained vibrational frequencies as depicted in Fig. 9.

Table 5
Experimental and calculated values of wavenumber for the selected vibrations of flavone hydrazones (Compound **3a** and **3j**).

Compound **3a** Main Assignments (%PED)	Vibrational Frequencies (cm^{-1}) Experimental	Theoretical	Compound **3j** Main Assignments (%PED)	Vibrational Frequencies (cm^{-1}) Experimental	Theoretical
νN–H (76)	3362	3213	νN–H (89)	3362	3218
νC–H (95)	3102	3208	νC–H (94)	3102	3207
νC=*N* (50)	1613	1577	νC=*N* (45)	1614	1572
νC=*O* (35)	1251	1252	νC=*O* (28)	1250	1250
νN–O (70)	1375	1341	νN–O (60)	1375	1340
νN–N (51)	1060	1051	νN–N (36)	1061	1024
νC–Cl (15)	763	734	νS-C (63), νS-O (78)	1215, 967	1108, 926
βHNN (41)	1645	1626	βHNN (22)	1644	1621
βHCC (72)	1330	1378	βHCC (83)	1375	1373
βCNO (39)	654	639	βHCH (74)	1533	1556
τHCCC (86)	830	857	τHCCC (84)	967	963
τHCCN (86)	1105	1088	τHCCN (60)	923	935
HNNC (32)	845	812	CCSN (56)	762	616

ν: stretching, β: in-plane bending, τ: torsional.

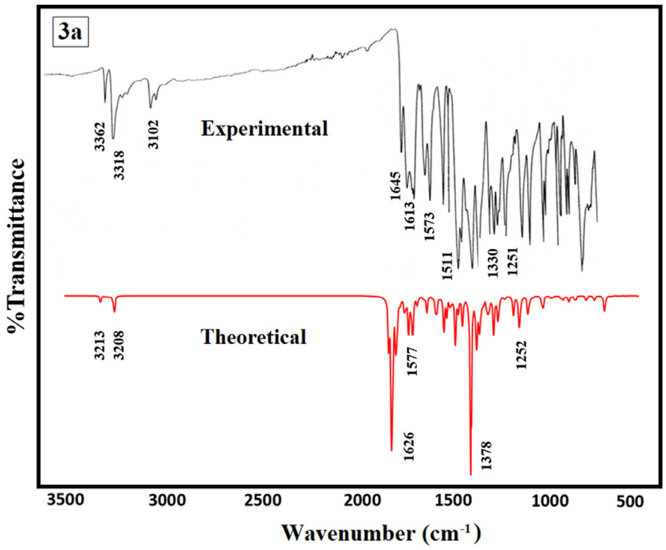

Fig. 8a. Experimental and DFT-B3LYP/321 g calculated IR spectra of representative compound (**3a**).

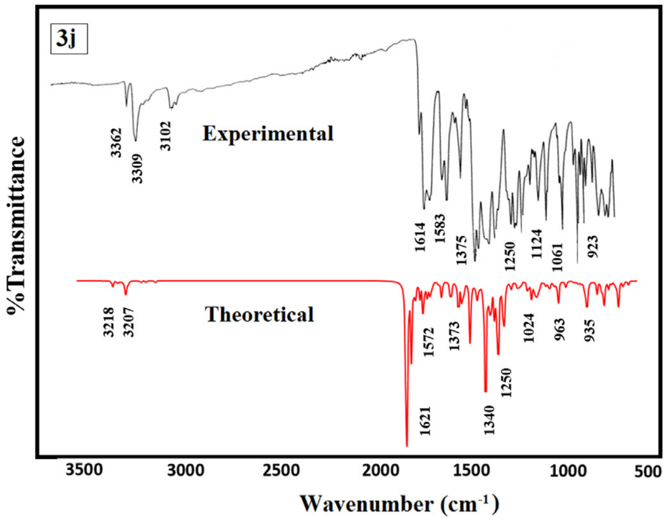

Fig. 8b. Experimental and DFT-B3LYP/321 g calculated IR spectra of representative compound (**3j**).

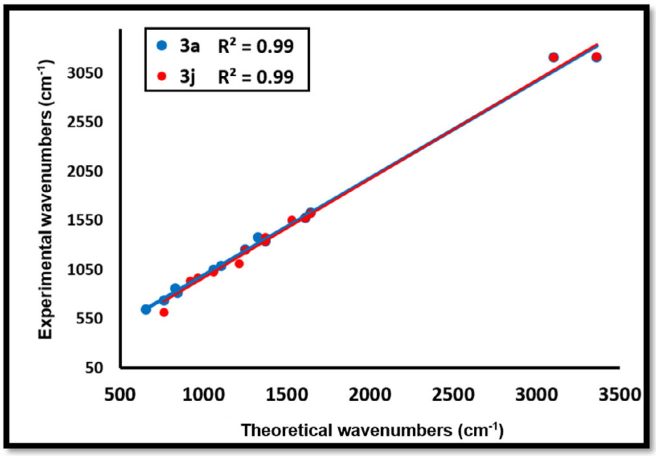

Fig. 9. Correlation diagram between the calculated and experimental wavenumbers of flavone hydrazone (**3a** and **3j**).

3.10. N–H vibrations

Generally, the N–H stretching vibrations are facilely determined by the apparition of a sharp peak at the highest wavenumbers. For the investigated flavone hydrazone molecules **3a** and **3j**, the symmetric stretching vibrations of N–H are located at 3362 cm^{-1} of both analogs. The calculated N–H stretching vibrations for hydrazone compounds **3a** and **3j** are both at 3213 and 3218 cm^{-1} using B3LYP methods with a 6–31G(d,p) basis set. The theoretically calculated N–H vibrations of hydrazone are the purest mode as evidenced from 76% and 89% of PED in compounds **3a** and **3j**, respectively.

3.11. C–H vibrations

The molecular structure of flavone-based hydrazones indicates the presence of the aromatic C–H stretching vibrations. The heteroaromatic structure shows the presence of C–H stretching vibrations in the region 3100–3000 cm^{-1} which is the characteristic region for the ready identification of C–H stretching vibrations [56, 57]. The B3LYP/6–31G(d,p) calculations give bands at 3208 cm^{-1} and 3207 cm^{-1} for **3a** and **3j** compounds, respectively, as CH modes. As indicated by PED, these modes involve an exact contribution of 95% and 94% suggesting that they are pure stretching modes. In this region, the bands are not affected remarkably by the nature of the substituent.

3.12. C = N and C-O vibrations

The bands in the region of 1640–1610 cm^{-1} are due to $C = N$ stretching vibrations, which shift the wavenumber and intensity in a coordination compound fashion depending on the neighboring group, conjugation effects, H-bonding and molecular tautomerism [56, 57]. The C–O vibrations were found at 1230–1250 cm^{-1}, which is normally the result of the combination of vibrational bands of other functional groups. The bands appearing in the IR spectrum at 1614, 1251 and 1250 cm^{-1} correspond to the stretching vibrations of the $C = N$ and C–O groups. The calculated bands are 1577 (50%) and 1252 (35%) cm^{-1} for compound **3a** and 1572 (45%) and 1215 (28%) cm^{-1} for compound **3j** at the B3LYP/6- 31G(d,p) level for the $C = N$ and C–O vibrational modes.

3.13. N–O and N-N vibrations

Generally, the N–O and N–N stretching modes of aromatic rings appeared between 1400 and 1000 cm^{-1}. Consequently, for the studied compounds **3a** and **3j**, the N–O stretching vibrations are observed at 1375 cm^{-1} for both analogs in the experimental IR spectrum and the N–N stretching vibrations are observed at 1060 and 1061 cm^{-1} for both analogs, respectively. Also, the aromatic $C = C$ stretching vibrations have appeared between 1625 and 1430 cm^{-1}. In flavone-based hydrazones, compounds **3a** and **3j,** the calculated band was found at 1341 (70%) and 1340 (60%) cm^{-1} for N–O and at 1051 (51%) and 1024 (36%) cm^{-1} for N–N band which nicely correlated with experimental values, respectively. As indicated by PED, these modes involve an exact contribution of $>$ 80% suggesting that they are pure stretching modes.

3.14. NNH and HCCN vibrations

Mostly, the NNH and HCCN bending and torsional modes of aromatic rings appeared between 1700 and 1120 cm^{-1}. Consequently, for the studied compounds **3a** and **3j**, the NNH bending vibrations are observed at 1645 and 1644 cm^{-1} respectively in the experimental IR spectrum and the HCCN torsional vibrations are observed at 1105 and 923 cm^{-1} for both analogs, respectively. Also, the aromatic $C = C$ stretching vibrations have appeared between 1625 and 1430 cm^{-1}. In flavone-based hydrazones, compounds **3a** and **3j,** the calculated band was found at 1626 (41%) and 1621 (22%) cm^{-1} for NNH and at 1088 (86%) and 935 (60%) cm^{-1} for the HCCN band which nicely correlated with experimental values, respectively.

3.15. C–X, C-S and S-O vibrations

The chlorine compound absorbs strongly in the region 770–670 cm^{-1} due to the C–Cl stretching vibrations and the sulfur compound absorbs in the region of 1225–920 cm^{-1} due to C–S and S–O. In the spectrum of compound **3a,** the (C–Cl) stretching vibration contributes to the bands computed at 763 cm^{-1} and in compound **3j** spectrum, the (S-C and S-O) stretching vibrations contribute to the bands calculated at 1108, 926 cm^{-1}, respectively. These results show excellent agreement with the assignment reported earlier. According to the calculated PED, the stretching (C–Cl) vibration in compound **3a** contributes 15% and compound **3j** contributes upto 78%.

4. Conclusions

In summary, we have designed, synthesized and characterized an interesting series of flavone-based hydrazones carrying distinct substitution patterns by utilizing the precedent procedure. The molecular structures of these analogs were characterized by different spectroscopic techniques. To illustrate structure-property relationships and the effect of different functionalities on the flavone scaffold, we have studied their emission and absorption properties in dilute solutions. A fluorescence study of these hydrazones in dilute CH_3CN solution showed a change from hypsochromic (blue) to bathochromic (red) shift. All the analogs showed amazing fluorescence properties and different maximal emission bands due to the unique nature of the substituents. This work also describes the electrochemical behavior of the hydrazones where quasi-reversible redox reactions have been demonstrated, and the electrode reaction has been regulated by the diffusion and adsorption methods. It has also been found that the presence of an EWG reduced the activity while an EDG enhanced the activity of the hydrazone derivatives. From these outcomes, it can be concluded that the position and nature of the substituents are two essential parameters influencing the electrochemical and photophysical properties. The CV results were further endorsed by the DFT study. The *in-silico* outcomes were in a great deal with the experimental findings. We are optimistic that the presented compounds may find promising applications as organic materials in electronics, and this will be the focus of our future research.

Credit author's statement

Meshari A. Alsharif: Data analysis and collection, software; **Nafeesa Naeem**: Experimental work performance, first-draft preparation**;** **Ehsan Ullah Mughal**: Main idea, supervision, final writing the manuscript**;** **Amina Sadiq**: Co-supervision, manuscript writing**;** **Rabab. S. Jassas:** Fluorescence analysis and interpretation**;** **Samia Kausar**: Performed DFT studies**;** **Ataf Ali Altaf**: Performed DFT studies**;** **Muhammad Naveed Zafar**: Mass spectrometry analysis and interpretation**;** **Amara Mumtaz:** Data analysis and collection, software**;** **Rami J. Obaid:** Data analysis and collection**;** **Reem I. Alsantali:** UV analysis and interpretation**;** **Safeer Ahmed:** Cyclic voltammetric analysis and interpretation**;** **Ishtiaq Ahmed:** NMR characterization**;** **Hatem M. Altass:** Data analysis and collection**;** **Saleh A. Ahmed:** Co-supervision and manuscript writing**.**

Declaration of Competing Interest

Declare that we have NO conflict of interest.

Acknowledgments

The authors would like to thank the Deanship of Scientific Research at Umm Al-Qura University for supporting this work under project no. 18-SCI-1-02-0006. The financial support by the Higher Education Commission of Pakistan (HEC) under Project No. (NRPU-6484) is gratefully acknowledged.

Supplementary materials

Supplementary material associated with this article can be found, in the online version, at doi:10.1016/j.molstruc.2021.130965.

References

[1] J. Ashraf, E.U. Mughal, A. Sadiq, N. Naeem, S.A. Muhammad, T. Qousain, M.N. Zafar, B.A. Khan, M. Anees, Design and synthesis of new flavonols as dual α-amylase and α-glucosidase inhibitors: structure-activity relationship, drug–likeness, *in vitro* and *in silico* studies, J. Mol. Struct. (2020) 128458.

[2] E.U. Mughal, A. Sadiq, M. Ayub, N. Naeem, A. Javid, S.H. Sumrra, M.N. Zafar, B.A. Khan, F.P. Malik, I. Ahmed, Exploring 3-Benzyloxyflavones as new lead cholinesterase inhibitors: synthesis, structure–activity relationship and molecular modelling simulations, J. Biomol. Struct. Dyn. (2020) 1–14.

[3] M. Singh, M. Kaur, O. Silakari, Flavones: an important scaffold for medicinal chemistry, Eur. J. Med. Chem. 84 (2014) 206–239.

[4] H. Adibi, J.S. Mojarrad, H. Asgharloo, G. Zarrini, Synthesis, *in vitro* antimicrobial and antioxidant activities of chalcone and flavone derivatives holding allylic substitutions, Med. Chem. Res. 20 (8) (2011) 1318–1324.

[5] W.F. Hodnick, E.B. Mllosavljevic, J.H. Nelson, R.S. Pardini, Electrochemistry of flavonoids: relationships between redox potentials, inhibition of mitochondrial respiration, and production of oxygen radicals by flavonoids, Biochem. Pharmacol. 37 (13) (1988) 2607–2611.

[6] R. de Queiroz Ferreira, S.J. Greco, M. Delarmelina, K.C. Weber, Electrochemical quantification of the structure/antioxidant activity relationship of flavonoids, Electrochim. Acta 163 (2015) 161–166.

[7] I.B. Masesane, A comprehensive review of the oxidative cyclisation of 2’-hydroxychalcones to aurones and flavones, Int. J. Chem. Stud. 3 (3) (2015) 53–59.

[8] R.K.Y. Shaikh, G. Nazeruddin, Synthesis of flavone skeleton by different methods, Orient. J. Chem. 29 (4) (2014) 1475–1487.

[9] (a) E.U. Mughal, M. Ayaz, Z. Hussain, A. Hasan, A. Sadiq, M. Riaz, A. Malik, S. Hussain, M.I. Choudhary, Synthesis and antibacterial activity of substituted flavones, 4-thioflavones and 4-iminoflavones, Bioorg. Med. Chem. 14 (14) (2006) 4704–4711; (b) S. Imran, M. Taha, N.H. Ismail, S.M. Kashif, F. Rahim, W. Jamil, M. Hariono, M. Yusuf, H. Wahab, Synthesis of novel flavone hydrazones: *in-vitro* evaluation of α-glucosidase inhibition, QSAR analysis and docking studies, Eur. J. Med. Chem. 105 (2015) 156–170; (c) A.K. Verma, R. Pratap, Chemistry of biologically important flavones, Tetrahedron 68 (41) (2012) 8523–8538; (d) S. Patel, U. Shah, Synthesis of flavones from 2-hydroxyacetophenone and aromatic aldehyde derivatives by conventional methods and green chemistry approach, Asian J. Pharmaceut. Clin. Res. 10 (2) (2017) 570–589; (e) D.C.S. Lima, C.R. Vale, J.H. Véras, A. Bernardes, C.N. Pérez, L. Chen-Chen, Absence of genotoxic effects of the chalcone (E)-1-(2-hydroxyphenyl)-3-(4-methylphenyl)-prop-2-en-1-one) and its potential chemoprevention against DNA damage using *in vitro* and *in vivo* assays, PLoS One 12 (2) (2017) 0171224; (f) M. Cabrera, M. Simoens, G. Falchi, M.L. Lavaggi, O.E. Piro, E.E. Castellano, A. Vidal, A. Azqueta, A. Monge, A.L. de Cerain, Synthetic chalcones, flavanones, and flavones as antitumoral agents: biological evaluation and structure–activity relationships, Bioorg. Med. Chem. 15 (10) (2007) 3356–3367; (g) J. Chen, C.-F. Liu, G.-W. Rao, Progress in the synthesis, angiogenesis activity and mechanism of chalcone derivatives, Mini Rev. Org. Chem. 17 (7) (2020) 814–827; (h) R.S. Joshi, P.G. Mandhane, S.D. Diwakar, S.K. Dabhade, C.H. Gill, Synthesis, analgesic and anti-inflammatory activities of some novel pyrazolines derivatives, Bioorg. Med. Chem. Lett. 20 (12) (2010) 3721–3725; (i) M. Cabrera, M.L. Lavaggi, F. Croce, L. Celano, L. Thomson, M. Fernández, C. Pintos, S. Raymondo, M. Bollati, A. Monge, Identification of chalcones as *in vivo* liver monofunctional phase II enzymes inducers, Bioorg. Med. Chem. 18 (14) (2010) 5391–5399; (j) J. Horkaew, S. Chantrapromma, N. Saewan, H.-K. Fun, (E)-3-(4-Ethoxyphenyl)-1-(2-hydroxyphenyl) prop-2-en-1-one, Acta Crystallographica Section E 66 (9) (2010) 2346–2347; (k) R. Baskar, C. Baby, M. Moni, K. Subramanian, Synthesis, characterization and dynamic NMR studies of a novel chalcone based N-substituted morpholine derivative, J. Mol. Struct. 1040 (2013) 90–97; (l) D. Coutinho, P. Fernandes, Synthesis and biological activity of some 2-Aryl-4H-L-benzopyran-4-ones, J. Indian Chem. Soc. 69 (5) (1992) 265–267; (m) Y. Hoshino, N. Takeno, Ortho substituent effect of the side-chain phenyl group on the dehydrogenation of flavanones with 2, 3-dichloro-5, 6-dicyano-p-benzoquinone, Bull. Chem. Soc. Jpn. 60 (12) (1987) 4468–4470; (n) V.N. Badavath, S. Ciftci-Yabanoglu, S. Bhakat, A.K. Timiri, B.N. Sinha, G. Ucar, M.E. Soliman, V. Jayaprakash, Monoamine oxidase inhibitory activity of 2-aryl-4H-chromen-4-ones, Bioorg. Chem. 58 (2015) 72–80; (o) M. Gharpure, R. Choudhary, V. Ingle, H. Juneja, Synthesis of new series of 3-hydroxy/acetoxy-2-phenyl-4H-chromen-4-ones and their biological importance, J. Chem. Sci. 125 (3) (2013) 575–582; (p) A.M. Sobottka, W. Werner, G. Blaschke, W. Kiefer, U. Nowe, G. Dannhardt, E.E. Schapoval, E.P. Schenkel, G.K. Scriba, Effect of flavonol derivatives on the carrageenin-induced paw edema in the rat and inhibition of cyclooxygenase-1 and 5-lipoxygenase *in vitro*, Arch. Pharm. (Weinheim) 333 (7) (2000) 205–210.

[10] A. Gul, Z. Akhter, F. Perveen, S. Kalsoom, F.L. Ansari, M. Siddiq, Molecular docking and quantitative structure activity relationship (QSAR) studies of some newly synthesized poly (azomethine) esters, Int. J. Polym. Sci. 8 (2) (2019) 346–350.

[11] S. Patil, P. Utale, S. Gholse, S. Thakur, S. Pande, Synthesis, characterization and antimicrobial activity of 6-bromo-4-methoxy-4-(substituted phenyl) iminoflavone, J. Chem. Pharm. Res. 4 (1) (2012) 501–507.

[12] A. Gomes, E. Fernandes, M.B.Q. Garcia, A.M. Silva, D.C. Pinto, C.M. Santos, J.A. Cavaleiro, J.L. Lima, Cyclic voltammetric analysis of 2-styrylchromones: relationship with the antioxidant activity, Bioorg. Med. Chem. 16 (17) (2008) 7939–7943.

[13] A. Abdelmadjid, D. Haffar, F. Benghanem, S. Ghedjati, L. Toukal, V. Dorcet, R. Bourzami, Synthesis, crystal structure, electrochemical, theoretical studies and antioxidant activities of new Schiff base, J. Mol. Struct. (2020) 129368.

[14] A.M. Fathi, H.S. Mandour, E. HassaneAnouar, Characteristics of multidentate schiff base ligand and its complexes using cyclic voltammetry, fluorescence, antimicrobial behavior and DFT-calculations, J. Mol. Struct. 1224 (2020) 129263.

[15] F. Hueso-Urena, N.A. Illán-Cabeza, M.N. Moreno-Carretero, A. Penas-Chamorro, Ni (II), Cu (II), Zn (II) and Cd (II) complexes with dinegative N, N, O-tridentate uracil-derived hydrazones, Acta Chim. Slov. 47 (4) (2000) 481–488.

[16] J. Ashraf, E.U. Mughal, A. Sadiq, M. Bibi, N. Naeem, A. Ali, A. Massadaq, N. Fatima, A. Javid, M.N. Zafar, Exploring 3-hydroxyflavone scaffolds as mushroom tyrosinase inhibitors: synthesis, X-ray crystallography, antimicrobial, fluorescence behaviour, structure-activity relationship and molecular modelling studies, J. Biomol. Struct. Dyn. (2020) 1–16.

[17] A. Sykula, A. Kowalska-Baron, A. Dzeikala, A. Bodzioch, E. Lodyga-Chruscinska, An experimental and DFT study on free radical scavenging activity of hesperetin Schiff bases, Chem. Phys. 517 (2019) 91–103.

[18] N. Uddin, F. Rashid, S. Ali, S.A. Tirmizi, I. Ahmad, S. Zaib, M. Zubair, P.L. Diaconescu, M.N. Tahir, J. Iqbal, Synthesis, characterization, and anticancer activity of Schiff bases, J. Biomol. Struct. Dyn. 38 (11) (2020) 3246–3259.

[19] N. Beyazit, D. Çakmak, C. Demetgül, Chromone-based Schiff base metal complexes as catalysts for catechol oxidation: synthesis, kinetics and electrochemical studies, Tetrahedron 73 (19) (2017) 2774–2779.

[20] H.R. Zare, N. Nasirizadeh, A study of the electrochemical behavior of hematoxylin as an important bioactive flavonoid, Electrochim. Acta 56 (11) (2011) 3920–3925.

[21] (a) X. Zhang, Y.-H. Jin, H.-X. Diao, F.-S. Du, Z.-C. Li, F.-M. Li, Synthesis of bismaleimides bearing electron-donating chromophores and their fluorescence behavior during copolymerization, Macromolecules 36 (9) (2003) 3115–3127; (b) S. Tang, W. Li, F. Shen, D. Liu, B. Yang, Y. Ma, Highly efficient deep-blue electroluminescence based on the triphenylamine-cored and peripheral blue emitters with segregative HOMO–LUMO characteristics, J. Mater. Chem. 22 (10) (2012) 4401–4408.

[22] R. Pohl, V.A. Montes, J. Shinar, P. Anzenbacher, Red− green− blue emission from Tris (5-aryl-8-quinolinolate) Al (III) complexes, J. Org. Chem. 69 (5) (2004) 1723–1725.

[23] J.M. Bobbitt, J.P. Willis, Electrochemistry of natural products. Oxidative decarboxylation of some tetrahydro-. beta.-carbolinecarboxylic acids, J. Org. Chem. 45 (10) (1980) 1978–1984.

[24] D. Tarinc, B. Dogan-Topal, M. Dolaz, A. Golcu, S.A. Ozkan, Synthesis, characterization, biological activity and voltammetric behavior and determination of cefaclor metal complexes, Curr. Anal. Chem. 6 (4) (2010) 316–328.

[25] R.F. De Souza, W.F. De Giovani, Synthesis, spectral and electrochemical properties of Al (III) and Zn (II) complexes with flavonoids, Spectrochim. Acta Part A 61 (9) (2005) 1985–1990.

[26] R.F. De Souza, E.M. Sussuchi, W.F. De Giovani, Synthesis, electrochemical, spectral, and antioxidant properties of complexes of flavonoids with metal ions, Synth. React. Inorg. Met. Org. Chem. 33 (7) (2003) 1125–1144.

[27] S. Güney, G. Yildiz, A. Capan, T. Ozturk, Evaluation of the electrochemical properties of 3-hydroxyflavone using voltammetric methods, Electrochim. Acta 55 (9) (2010) 3295–3300.

[28] K. Harisha, B.K. Swamy, E.E. Ebenso, Poly (glycine) modified carbon paste electrode for simultaneous determination of catechol and hydroquinone: a voltammetric study, J. Electroanal. Chem. 823 (2018) 730–736.

[29] K. Harisha, B.K. Swamy, P. Ganesh, H. Jayadevappa, Electrochemical oxidation of haematoxylin at poly (alanine) modified carbon paste electrode: a cyclic voltammetric study, J. Electroanal. Chem. 832 (2019) 486–492.

[30] K.V. Harisha, B.E.K. Swamy, P.S. Ganesh, H. Jayadevappa, An electrochemical sensor for the determination of 5-amino salicylic acid at poly (alanine) modified carbon paste electrode: a cyclic voltammetric study, Anal. Bioanal. Electrochem. 10 (10) (2018) 1273–1287.

[31] E.I. Korotkova, O.A. Voronova, E.V. Dorozhko, Study of antioxidant properties of flavonoids by voltammetry, J. Solid State Electrochem. 16 (7) (2012) 2435–2440.

[32] A. Masek, E. Chrzescijanska, M. Zaborski, Characteristics of curcumin using cyclic voltammetry, UV–vis, fluorescence and thermogravimetric analysis, Electrochim. Acta 107 (2013) 441–447.

[33] A. Masek, E. Chrzescijanska, M. Zaborski, Electrooxidation of morin hydrate at a Pt electrode studied by cyclic voltammetry, Food Chem. 148 (2014) 18–23.

[34] F. Kolcu, D. Erdener, İ. Kaya, A Schiff base based on triphenylamine and thiophene moieties as a fluorescent sensor for Cr (III) ions: synthesis, characterization and fluorescent applications, Inorganica Chim Acta 509 (2020) 119676.

[35] H. Vural, Ö. İdil, Synthesis, spectroscopic investigation and biological activities of copper (II) complex of 2-(2, 4-difluorophenyl) pyridine: a combined theoretical and experimental study, J. Mol. Struct. 1177 (2019) 242–248.

[36] A. Mishra, E. Mena-Osteritz, P. Bäuerle, Synthesis, photophysical and electrochemical characterization of terpyridine-functionalized dendritic oligothiophenes and their Ru (II) complexes, Beilstein J. Org. Chem. 9 (1) (2013) 866.

[37] (a) A.S. Girgis, A.H. Basta, H. El-Saied, M.A. Mohamed, A.H. Bedair, A.S. Salim, Synthesis, quantitative structure–property relationship study of novel fluorescence active 2-pyrazolines and application, R. Soc. Open Sci. 5 (3) (2018) 171964; (b) M. Soltani, R. Minakar, H.R. Memarian, H. Sabzyan, Cyclic voltammetric study of 3, 5-diaryl-1-phenyl-2-pyrazolines, J. Phys. Chem. A 123 (13) (2019) 2820–2830; (c) V. Ramkumar, P. Kannan, Highly fluorescent semiconducting pyrazoline materials for optoelectronics, Opt. Mater. (Amst) 46 (2015) 605–613.

[38] (a) A.M. Polgar, J. Poisson, N.R. Paisley, C.J. Christopherson, A.C. Reyes, Z.M. Hudson, Blue to yellow thermally activated delayed fluorescence with quantum yields near unity in acrylic polymers based on D− π −A pyrimidines, Macromolecules 53 (6) (2020) 2039–2050; (b) P. Ganesan, R. Ranganathan, Y. Chi, X.K. Liu, C.S. Lee, S.H. Liu, G.H. Lee, T.C. Lin, Y.T. Chen, P.T. Chou, Functional pyrimidine-based thermally activated delay fluorescence emitters: photophysics, mechanochromism, and fabrication of organic light-emitting diodes, Chemistry–A Eur. J. 23 (12) (2017) 2858–2866.

[39] (a) D.-D. Li, J.-L. Tian, W. Gu, X. Liu, S.-P. Yan, A novel 1, 2, 4-triazole-based copper (II) complex: synthesis, characterization, magnetic property and nuclease activity, J. Inorg. Biochem. 104 (2) (2010) 171–179; (b) Z.-H. Xing, J.-Y. Zhuang, X.-P. Xu, S.-J. Ji, W.-M. Su, Z. Cui, Novel oxazole-based emit-

ters for high efficiency fluorescent OLEDs: synthesis, characterization, and optoelectronic properties, Tetrahedron 73 (15) (2017) 2036–2042.

[40] İ. Kaya, M. Yıldırım, A. Avcı, Synthesis and characterization of fluorescent polyphenol species derived from methyl substituted aminopyridine based Schiff bases: the effect of substituent position on optical, electrical, electrochemical, and fluorescence properties, Synth. Met. 160 (9–10) (2010) 911–920.

[41] E.U. Mughal, M. Mirzaei, A. Sadiq, S. Fatima, A. Naseem, N. Naeem, N. Fatima, S. Kausar, A.A. Altaf, M.N. Zafar, Terpyridine-metal complexes: effects of different substituents on their physico-chemical properties and density functional theory studies, R. Soc. Open Sci. 7 (11) (2020) 201208.

[42] A. Masek, M. Zaborski, E. Chrzescijanska, Electrooxidation of flavonoids at platinum electrode studied by cyclic voltammetry, Food Chem. 127 (2) (2011) 699–704.

[43] A.A. Altaf, S. Kausar, A. Badshah, Spectral calculations with DFT, density functional calculations–recent progresses of theory and application (2018) 13.

[44] A. Frisch, Gaussian 09w reference, Wallingford, USA, 25p (2009).

[45] B. Lal, A. Kanwal, A.A. Altaf, A. Badshah, F. Asghar, S. Akhter, S. Ullah, S.I. Khan, M.N. Tahir, Synthesis, crystal structure, spectral and electrochemical characterization, DNA binding and free radical scavenging studies of ferrocene-based thioureas, J. Coord. Chem. 72 (14) (2019) 2376–2392.

[46] M. Marinov, S. Minchev, N. Stoyanov, G. Ivanova, M. Spassova, V. Enchev, Synthesis, spectroscopic characterization and ab initio investigation of thioanalogues of spirohydantoins, Croat. Chem. Acta 78 (1) (2005) 9–16.

[47] A.A. Altaf, A. Shahzad, Z. Gul, S.A. Khan, A. Badshah, M.N. Tahir, Z.I. Zafar, E. Khan, Synthesis, crystal structure, and DFT calculations of 1, 3-diisobutyl thiourea, J. Chem. (2015) 2015.

[48] F. Asghar, S. Fatima, S. Rana, A. Badshah, I.S. Butler, M.N. Tahir, Synthesis, spectroscopic investigation, and DFT study of N, N′-disubstituted ferrocene-based thiourea complexes as potent anticancer agents, Dalton Trans. 47 (6) (2018) 1868–1878.

[49] J. Aihara, Reduced HOMO− LUMO gap as an index of kinetic stability for polycyclic aromatic hydrocarbons, J. Phys. Chem. A 103 (37) (1999) 7487–7495.

[50] S.H. Sumrra, S. Kausar, M.A. Raza, M. Zubair, M.N. Zafar, M.A. Nadeem, E.U. Mughal, Z.H. Chohan, F. Mushtaq, U. Rashid, Metal based triazole compounds: their synthesis, computational, antioxidant, enzyme inhibition and antimicrobial properties, J. Mol. Struct. 1168 (2018) 202–211.

[51] K. Benbouguerra, N. Chafai, S. Chafaa, Y.I. Touahria, H. Tlidjane, New α-Hydrazinophosphonic acid: synthesis, characterization, DFT study and *in silico* prediction of its potential inhibition of SARS-CoV-2 main protease, J. Mol. Struct. 1239 (2021) 130480.

[52] J. Haruyama, T. Ikeshoji, M. Otani, Electrode potential from density functional theory calculations combined with implicit solvation theory, Phys. Rev. Mater. 2 (9) (2018) 095801.

[53] D. Suresh, M. Amalanathan, S. Sebastian, D. Sajan, I.H. Joe, V.B. Jothy, I. Nemec, Vibrational spectral investigation and natural bond orbital analysis of pharmaceutical compound 7-Amino-2, 4-dimethylquinolinium formate–DFT approach, Spectrochim. Acta Part A 115 (2013) 595–602.

[54] R. Carbó-Dorca, P. Bultinck, Quantum mechanical basis for Mulliken population analysis, J. Math. Chem. 36 (3) (2004) 231–239.

[55] (a) F.C. Chahar, P.E. Alvarez, C. Zampini, M.I. Isla, S.A. Brandán, Experimental and DFT studies on 2′,4′-dihydroxychalcone, a product isolated from *Zuccagnia punctata Cav.*(Fabaceae) medicinal plant, J. Mol. Struct. 1201 (2020) 127221; (b) K. Karrouchi, S.A. Brandán, Y. Sert, M. El Karbane, S. Radi, M. Ferbinteanu, Y. Garcia, Synthesis, structural, molecular docking and spectroscopic studies of (E)-N'-(4-methoxybenzylidene)-5-methyl-1H-pyrazole-3-carbohydrazide, J. Mol. Struct. 1225 (2021) 129072.

[56] A. Esme, S. Sagdinc, Theoretical Studies of Molecular Structures, Infrared Spectra, NBO and NLO Properties of Some Novel 5-arylazo-6-hydroxy-4-phenyl-3-cyano-2-pyridone Dyes, Acta Physica Polonica, A 130 (6) (2016).

[57] H. Sahebalzamani, F. Salimi, E. Dornapour, Theoretical studies of structure, spectroscopy, and properties of a new hydrazine derivative, J. . 13 (3) (2013).